Combustion and Flame 183 (2017) 283–298

Contents lists available at ScienceDirect

Combustion and Flame

journal homepage: www.elsevier.com/locate/combustflame

Importance of turbulence-chemistry interactions at low temperature engine conditions

Prithwish Kundu*, Muhsin M Ameen, Sibendu Som

Energy Systems, Argonne National Laboratory, 9700 S. Cass Av., Lemont, IL, USA

ARTICLE INFO

Article history:
Received 16 December 2016
Revised 22 May 2017
Accepted 22 May 2017
Available online 8 June 2017

Keywords:
Low temperature combustion
ECN spray A
Flamelets
LES

ABSTRACT

The role of turbulence-chemistry interaction in autoignition and flame stabilization is investigated for spray flames at low temperature combustion (LTC) conditions by performing high-fidelity three-dimensional computational fluid dynamics (CFD) simulations. A recently developed Tabulated Flamelet Model (TFM) is coupled with a large eddy simulation (LES) framework and validated across a range of Engine Combustion Network (ECN) ambient temperature conditions for n-dodecane fuel. High resolution grids with 0.0625 mm minimum cell size and 25 million total cell count are implemented using adaptive mesh refinement over the spray and combustion regions. Simulations with these grids and multiple LES realizations, with a 103 species n-dodecane mechanism show good agreement with experimental data for all the ambient conditions investigated. This modeling approach with the computational cost advantage of tabulated chemistry is then extended towards understanding the auto-ignition and flame stabilization at an ambient temperature of 750 K. These low temperature conditions lead to substantially higher ignition delays and flame liftoff lengths, and significantly leaner combustion compared to conventional high temperature diesel combustion. These conditions also require the simulations to span significantly larger temporal and spatial dimensions thereby increasing the computational cost. The TFM approach is able to capture autoignition and flame liftoff length at the low temperature conditions. Significant differences with respect to mixing, species formation and flame stabilization are observed under low temperature compared to conventional diesel combustion. At higher ambient temperatures, formation of formaldehyde is observed in the rich region (phi > 1) followed by the formation of OH in the stoichiometric regions. Under low temperature conditions, formaldehyde is observed to form at leaner regions followed by the onset of OH formation in significantly lean regions of the flame. Qualitative differences between species formation and transient flame development for the high and low temperature conditions are presented. The two stage ignition process is further investigated by studying the species formation in mixture fraction space by solving 1D flamelet equations for different scalar dissipation rates and homogeneous reactor assumption. Results show that scalar dissipation causes these radicals to diffuse within the mixture fraction space. This significantly enhances ignition and plays a dominant role at such low temperature conditions which cannot be captured by the homogeneous reaction assumption based model.

1. Introduction

Compression ignition engines will continue to play a dominant role in heavy duty applications due to their higher efficiency and power density. Considerable research effort has been directed towards improving their efficiency and reducing emissions. The traditional diesel engine strategy is characterized by mixing-controlled combustion and relatively high in-cylinder temperatures leading to a NOx-soot tradeoff. Reducing the overall temperature of combustion by employing lean mixtures has been the main strategy towards developing future engine concepts like Homogeneous Charge Compression Ignition, Premixed Charge Compression Ignition, Gasoline Compression Ignition and Lean Lifted Flame Combustion (LLFC) [1]. Autoignition at such conditions is a strong function of the chemical kinetics and turbulence-chemistry interactions. As a result, combustion phasing has proved to be a major challenge towards the development and application of these technologies. Numerical studies can be used as a tool to understand the mechanisms controlling the autoignition and flame stabilization processes resulting in an improved implementation of low temperature combustion strategies (LTC) in engines.

While a number of studies have been carried out in the recent past to understand the fundamentals of autoignition and flame stabilization at engine relevant temperature conditions, few studies

* Corresponding author. Abstract
E-mail address: pkundu@ncsu.edu (P. Kundu).

http://dx.doi.org/10.1016/j.combustflame.2017.05.025
0010-2180/

have also focused on low temperature conditions that may be relevant towards future low-temperature engine concepts. Bansal et al. [2] studied auto-ignition of hydrogen-air premixed mixtures using two dimensional Direct Numerical Simulation (DNS) over a temperature range of 1033–1116 K. The mixtures were subjected to different levels of thermal and equivalence ratio stratification. The results show that ignition delay and heat release rate pattern have a strong dependency on the stratification. Mukhopadhyay and Abraham [3] modeled an n-heptane mixing layer at 40 bar pressure and 1000 K ambient temperature using two-dimensional DNS. Higher scalar dissipation rates in presence of higher compositional stratification led to an increase of ignition delay. In case of lower compositional gradients, higher scalar dissipation rates led to reduction in ignition delays. In a later study [4], the effect of heat release on evolution of scalar dissipation rate was studied. Borghesi et al. [5] carried out DNS of an igniting n-heptane spray at 24 bar pressure and 1000 K ambient temperature. Ignition kernels were observed in regions of lower scalar dissipation rate and mixture fractions corresponding to the most reactive mixture fraction from homogeneous reactor simulations. Krisman et al. [6] studied the two stage ignition process of a mixing layer with Dimethyl Ether (DME) and air at 40 atm and 900 K using 2D DNS. The study identified a cool flame propagation and its impact on high temperature ignition. It was observed that the high temperature ignition spots do not correspond to the most reactive mixture fraction obtained from the homogeneous reactor assumption. The first stage ignition was observed to be shorter, and, the cool flame propagates much faster into the rich regions as compared to the homogeneous reactor predictions. This is followed by the shortening of main ignition and formation of high temperature kernels. Thus, the scalar dissipation causes a reduction in the main, i.e., high temperature ignition delay for these conditions that are characterized by a two stage ignition, negative temperature coefficient (NTC) chemistry and low temperature chemistry. Dahms et al. [7] carried out similar studies in 1D flamelets and showed the influence of the first stage ignition on the main ignition. The analysis also showed the applicability of the flamelet concept for the entire ignition process for the Spray A conditions.

Three-dimensional DNS of a turbulent lifted DME jet flame at 5 atm ambient pressure by Minamoto and Chen [8] showed the influence of two stage ignition, NTC chemistry and turbulence-chemistry interactions on flame propagation and highlighted the need to account for turbulence-chemistry interaction (TCI) in Reynolds-Averaged Navier–Stokes (RANS) simulations and large-eddy simulations (LES). Borghesi et al. [9] extended this study to 3D DNS of n-dodecane mixing layers at an ambient pressure of 25 bar. Stratification of mixture fraction was shown to have a strong influence on low temperature reactions. For the parameters and thermodynamic conditions considered in their study, the scalar dissipation did not cause a reduction of the main ignition delay. This observation with respect to the main ignition was not same as that observed by Krisman et al. [6]. Dahms et al. [10] solved the 1D flamelet equations coupled with a detailed 2755 species n-dodecane mechanism [11] at the standard Spray A condition of the Engine Combustion Network (ECN) characterized by 60 bar and 900 K ambient pressure and temperature, respectively. Comparative 1D studies with homogeneous reactor ignition delays showed that increase in scalar dissipation rate reduces the ignition delay and shifts the ignition location to richer regions.

The fundamental studies using DNS illustrate the coupled effect of chemistry and turbulence on auto ignition and flame stabilization. The chemistry mechanisms also need to capture the two stage ignition process and predict the low temperature species. The diffusion and transport of these low temperature species have a significant influence on the main ignition process. However, such high fidelity studies cannot span the time scales, length scales and Reynolds numbers encountered in an actual engine due to their high computational costs. This motivates the use of LES to get an understanding of these processes in engines. LES of igniting n-dodecane sprays that mimic diesel engine conditions (ECN spray A) have been reported in some studies. Pei et al. [12–14] implemented a homogeneous reactor combustion model and a multi-zone framework along with a 103 species n-dodecane mechanism [15] within a LES framework over a range of ambient temperatures and oxygen concentrations [12]. A minimum grid size of 0.0625 mm with approximately 22 million cells was found to be sufficient for these conditions. A similarity index analysis was used to find out the minimum number of LES realizations that are required to obtain statistically converged predictions. Quantitative and qualitative data from the simulations matched the experimental measurements over the range of investigated conditions. Ameen et al. [16] showed that a combination of azimuthal and ensemble averaging can be used to reduce the total number of LES realizations. Wehrfritz et al. [17] implemented the Flamelet Generated Manifold (FGM) combustion modeling approach to model the ECN spray A over a range of oxygen concentrations with multiple realizations for the 15% oxygen condition and a single realization for the other conditions. A 0.0625 mm minimum cell size mesh near the nozzle with 11 million cells was used in this study. Two different n-dodecane chemistry mechanisms were compared with respect to autoignition, flame stabilization and species formation. Qualitative results showed good agreement between simulation and experiments with respect to formation of CH_2O. Flame liftoff length from simulations was over predicted for the higher oxygen concentration. Ameen et al. [18] recently implemented the Tabulated Flamelet Model (TFM) within the LES framework and validated it against different ambient temperature conditions for a single LES realization and compared the results against the homogeneous reactor combustion model for an ambient temperature range of 800 to 1100 K. The model was able to predict the autoignition and flame liftoff length trends accurately. Qualitative data showed the formation of ignition kernels and transient flame development and stabilization under engine conditions. The high fidelity LES simulations have been limited to the range of 800 to 1100 K ambient temperature conditions with single injection. The one notable exception is the recent study by Blomberg et al. [19] who carried out simulations of split injection at 900 and 750 K ambient temperatures using the CMC combustion model coupled with LES with a relatively coarse mesh and minimum cell size of 0.125 mm. The total simulation duration was 1.5 ms with each injection spanning 0.5 ms separated by a dwell time of 0.5 ms. The model was able to capture the soot formation, intermediate species and combustion recession accurately. The availability of spray flame diagnostics data under diesel-engine relevant conditions, courtesy of the ECN, has led to several LES studies of the ECN sprays [20–23]. These studies have greatly increased our understanding of the autoignition, flame development and flame stabilization mechanisms under these conditions. Although these LES studies provide slightly conflicting explanations regarding the flame stabilization mechanism for these spray flames, most of these studies are able to predict the flame lift-off lengths accurately despite using different TCI models. It could be hypothesized that if the LES setup is able to predict the flow and mixing field correctly, and the grid is sufficiently resolved, TCI only plays a minor role in determining the flame lift-off length. However, these observations may only not hold true for LTC conditions, where the ignition delays are long, and the turbulent diffusion of intermediary species can strongly affect the autoignition behavior.

Over the past years, a number of RANS simulations encompassing a variety of combustion models and chemistry mechanisms have been carried out to model igniting spray flames at diesel engine conditions. Pei *et al.* carried out RANS simulations using the

transported PDF method [24–27]. The Conditional Moment Closure model was used to model igniting n-heptane sprays [28–30]. The tabulated FGM method was implemented in a number of spray flame studies [20,31–33] as well as single phase jet flames [34]. The unsteady flamelet progress variable method has also been used in some studies [35–37]. The FGM and UFPV approach use the progress variable concept to account for the unsteady chemistry within a manifold. Within the flamelet modeling framework, apart from tabulated methods, in-situ flamelet solvers, i.e., the Representative Interactive Flamelet (RIF) model was implemented to model igniting sprays over a range of conditions [38–48]. Pal et al. carried out engine simulations in a RANS framework with the RIF and homogeneous reactor model and reported a decrease in ignition delay due to the diffusion in mixture fraction space for the RIF model [49]. In a recent study the authors presented a model formulation for tabulated flamelets without using a progress variable method, based on the structure of the RIF model [50]. The computational costs were significantly lower compared to the RIF model. These studies were carried out for RANS simulations. Another version of the model without history effects i.e., the Tabulated Flamelet Model (TFM) was validated in RANS and LES simulations with a single realization at engine conditions [18,51]. Most of the non-premixed flame studies have been carried out for the 800 to 1100 K range. To the best of the authors' knowledge, detailed simulation studies on spray flames at 750 K have not been reported. This case is characterized by substantially longer ignition delay and injection durations which also implies a substantially higher computational cost compared to the higher temperature cases. The 800–1100 K conditions are more representative of the typical mixing controlled diesel combustion. The lower ambient temperature (750 K) needs to be investigated with regard to mixing, autoignition, intermediate species and flame stabilization process with low-temperature combustion concepts in mind. The role of turbulence and low temperature chemistry needs to be investigated at such engine relevant low temperature conditions. Previous DNS studies have already shown that the diffusion of radicals for a two stage ignition process can lead to an enhancement of the high temperature ignition. However, for spray-flames the time and length scales cannot be accommodated in a DNS study. For such long injection duration cases characterized by large liftoff lengths, the mixing field at the time of ignition cannot be approximated *a priori* or represented by a mixing layer problem. As a result, LES coupled with extensively validated spray and combustion models need to be implemented to shed some light on the coupled effects of low temperature chemistry, two stage ignition process and turbulence. This forms the primary motivation for the current study. The objective is to develop and validate a robust LES approach with our previously published TFM using multiple realization methodology together with azimuthal averaging. This validated approach is then used to probe spray flames at LTC conditions which is the primary objective of the current study. The literature search demonstrates that this LTC condition has not been simulated with LES.

The first part of this study describes the model formulation and computational setup for the LES cases (Section 2). This is followed by the results from the TFM approach with multiple realizations and validation against experimental data for the 800–1100 K ambient temperature range (Section 3.1). The model is then validated for the LTC case of 750 K with respect to jet penetration, autoignition and flame stabilization. Quantitative and qualitative data is presented in Section. 3.2. This is followed by a comparative study and differences between the 900 K baseline Spray A case and the 750 K ambient temperature condition (Section 3.3). Finally, the role of TCI in autoignition is investigated at low temperature conditions for n-dodecane (Section 3.4) followed by the summary and conclusion in Section 4.

2. Model formulation

The flamelet approach consists of decoupling chemistry calculations from fluid flow. The 1D laminar counter flow diffusion flame shows that the species composition space can be expressed as a function of the mixing which is quantified using mixture fraction (Z) with most of the reactive zone in thin regions called laminar flamelets. The turbulent flame can be considered as an ensemble of laminar flamelets, which get wrinkled due to turbulence. Instead of solving chemistry in the physical space, it can be solved in the mixture fraction space thereby eliminating the need to solve for transport equation for each species. This reduces the overall stiffness of the system thereby increasing the computational efficiency. The Tabulated Flamelet Model (TFM) is based on the structure of the Representative Interactive Flamelet model coupled with tabulated chemistry. This framework has been discussed in detail and validated in Refs. [18,50]. Ameen et al. [18] validated the implementation of TFM within LES with a single realization and also compared the results with homogeneous reactor model. A brief description of the model is provided here.

2.1. Flamelet equations

The flamelet equations can be derived from the species transport and energy conservation equations by applying a coordinate transformation from physical space to mixture fraction [52]. These equations are shown in Eqs. (1) and (2).

$$\rho\frac{\partial Y_i}{\partial t} = \rho\frac{\chi}{2}\frac{\partial^2 Y_i}{\partial Z^2} + \dot{\omega}_i \tag{1}$$

$$\rho\frac{\partial T}{\partial t} - \rho\frac{\chi}{2}\frac{\partial^2 T}{\partial Z^2} - \rho\frac{\chi}{2}\left[\sum_i\left(\frac{C_{pi}}{Le_i}\frac{\partial Y_i}{\partial Z} + \frac{\partial C_{p,i}}{\partial Z}\right)\right]\frac{\partial T}{\partial Z} = \frac{1}{C_p}\left(\frac{\partial P}{\partial t} - \sum_i \dot{\omega}_i h_i\right) \tag{2}$$

In these equations Y_i is the mass fraction of species i, T is the temperature, ρ is the density, Z is the mixture fraction, χ is the scalar dissipation rate, and $\dot{\omega}_i$ is the chemical source term of species i. C_p is the specific heat and Le_i is the Lewis number which is assumed to be unity in this study.

The functional dependence of χ on Z is parametrized in terms of its stoichiometric value based on the following profile recommended by Peters [52].

$$\chi(Z) = \chi_{st}\frac{exp\left[-2\left(erfc^{-1}(2Z)\right)^2\right]}{exp\left[-2\left(erfc^{-1}(2Z_{st})\right)^2\right]} \tag{3}$$

In Eq. (3), st refers to the stoichiometric condition and χ_{st} refers to the scalar dissipation rate at the stoichiometric condition. The flamelet equations (1) and (2) are solved using the scalar dissipation rate profile described in Eq. (3). In Eq. (1), the term on the left hand side represents the unsteady species evolution. The ambient temperature of the combustion chamber is specified as the temperature of oxidizer in the flamelet equations. The ambient pressure is used as the pressure for the flamelet equations. The oxidizer composition for the flamelet equations $Y_i(Z=0)$ are specified based on the initial oxidizer composition of the combustion chamber. The first term on the right hand side ($\rho\frac{\chi}{2}\frac{\partial^2 Y_i}{\partial Z^2}$) accounts for species diffusion within the mixture fraction space and $\dot{\omega}_i$ is the species source term. In the absence of diffusion, i.e., $\chi = 0$, the equations represent a homogeneous reactor. The solution of flamelet equations for a given χ_{st} gives species as a function of mixture fraction

at each time step $Y_i(t, \tilde{Z})$. In order to consider the turbulent fluctuations, a presumed PDF approach is used in this study. A beta PDF is constructed based on mean mixture fraction ($\tilde{Z}$) and mixture fraction variance ($\widetilde{Z''^2}$) [53,54]. The species mass fraction for a given time, mixture fraction and mixture fraction variance can thus be calculated as: $\tilde{Y}_i = \tilde{Y}_i(t, \tilde{Z}, \widetilde{Z''^2})$. For a constant pressure case, this process can be repeated for different scalar dissipation rates and the chemistry in a turbulent flow can thus be expressed as a lower dimensional manifold with 4 dimensions as shown in Eq. (4). In case of varying pressures, the manifold needs to be extended with pressure as an additional dimension [20,32,51].

$$\tilde{Y}_i = \tilde{Y}_i\left(t, \tilde{Z}, \widetilde{Z''^2}, \chi_{st}\right) \tag{4}$$

2.2. Flamelet library generation

The flamelet equations were solved *a priori* for a range of the independent variables of the manifold. In this setup, sub-manifolds can be generated in parallel with no communication with the other processes. As a result, large chemistry mechanisms can be tabulated in relatively short wall clock times. A reduced skeletal mechanism with 103 species and 370 reactions for n-dodecane fuel was used to generate the 4 dimensional libraries for a given pressure [15,55]. Table resolution studies for these conditions have been carried out by the authors and reported in [51]. The libraries were constructed using 28 points in χ_{st}, 21 points in t, 120 points in $\tilde{Z}$ and 21 points in $\widetilde{Z''^2}$. In this work, the flamelet equations are based on the classical mixture fraction formulation based on the concept of gaseous counter-flow diffusion flames. A more detailed approach would be to model the effect of vaporization source terms by modifying the flamelet equations [56]. However, in these lifted flames this effect is not considered as the liquid lengths are significantly smaller than the liftoff height and its impact is assumed to be small on the overall results. The ideal gas equation of state was used to solve the flamelet equations for the results presented in this work. However, some more analysis were carried out by implementing the Peng–Robinson equation of state in the flamelet solver. The differences with respect to ideal gas were minimal. The implementation and results are described in detail in Appendix A.

2.3. Tabulated Flamelet Model (TFM)

The TFM model was coupled with the Converge [57] computational fluid dynamics (CFD) code [18,50,51]. The CFD code solves for the continuity, momentum, energy, mixture fraction and mixture fraction variance equations. The species mass fraction at each cell is calculated based on $t, \tilde{Z}, \widetilde{Z''^2}$ *and* χ_{st} at each cell. The scalar dissipation rate is modeled as [23]:

$$\tilde{\chi} = \widetilde{\chi_{SGS}} + \widetilde{\chi_{res}} = \frac{D_t}{\Delta^2}\widetilde{Z''^2} \; + \; 2D\left|\nabla\tilde{Z}\right|^2 \tag{5}$$

$\widetilde{\chi_{res}}$ and $\widetilde{\chi_{SGS}}$ are the resolved and sub grid scalar dissipation rates respectively and D_t is the turbulent diffusivity. In order to account for the spatial variation of χ_{st}, the approach of multiple flamelets suggested by Barths et al. [41] is implemented. Multiple flamelets are injected along with the fuel which are tracked in the domain by a marker equation for each flamelet (l) as shown in Eq. (6).

$$\frac{\partial\left(\bar{\rho}\widetilde{Z_l}\right)}{\partial t} + \frac{\partial\left(\bar{\rho}\tilde{u}_l\widetilde{Z_l}\right)}{\partial x_l} = \; - \frac{\partial\left(\bar{\rho}\widetilde{u''_l Z''_l}\right)}{\partial x_l} + \bar{S} \tag{6}$$

where

$$\widetilde{u''_l Z''_l} = -D_t \; \frac{\partial\tilde{Z}}{\partial x_i}$$

and $\bar{S}$ is the mixture fraction source term which is obtained from the evaporation of liquid fuel from the spray model.

The markers must also satisfy the following condition:

$$\tilde{Z} = \sum_{l=1}^{n}\widetilde{Z_l}, \tag{7}$$

where n is the number of flamelets. Each flamelet that has been injected into the computational domain has its own residence time, t_l and scalar dissipation rate, $\widehat{\chi_{st}}(l)$. The residence time of each flamelet is the time elapsed since its injection into the domain. The scalar dissipation rate for each flamelet is determined from Eq. (8) [44].

$$\widehat{\chi_{st}}(l) = \frac{\int_{\frac{\widetilde{Z}_l}{2}}^{\widetilde{Z}_l}\bar{\rho}\,\widetilde{\chi_{st}}^{\frac{3}{2}}\tilde{P}(Z_{st})dv}{\int_{\frac{\widetilde{Z}_l}{2}}^{\widetilde{Z}_l}\bar{\rho}\,\widetilde{\chi_{st}}^{\frac{1}{2}}\tilde{P}(Z_{st})dv}, \tag{8}$$

$$\text{Where} \quad \widetilde{\chi_{st}} = \tilde{\chi}\,\frac{f(Z_{st})}{\int_0^1 f(Z)P(Z)dZ} \tag{9}$$

$$\text{and} \quad f(Z) = exp\left[-2\left(erfc^{-1}(2Z)\right)^2\right] \tag{10}$$

Eq. (9) calculates the stoichiometric scalar dissipation rate at each cell of the CFD domain which has a mean mixture fraction and variance. Eq. (8) calculates the conditional scalar dissipation rate at Z_{st} for each flamelet. The domain averaged value is weighted with the area of stoichiometric mixture present per unit volume in the cell. $\widehat{\chi_{st}}(l)$ is the spatially averaged stoichiometric scalar dissipation rate for each flamelet. $P()$ is the presumed beta PDF used in Eqs. (8) and (9).

$$P(Z;x,t) = \frac{\tilde{Z}^{\alpha-1}\left(1-\tilde{Z}\right)^{\beta-1}}{\Gamma(\alpha)\Gamma(\beta)}\Gamma(\alpha+\beta)$$

$$\text{Where} \;\; \alpha = \tilde{Z}\gamma \;\; \text{and} \;\; \beta = (1-\tilde{Z})\gamma \;\; \text{and} \;\; \gamma = \frac{(\tilde{Z}(1-\tilde{Z})}{\widetilde{Z''^2}} - 1 \tag{11}$$

As shown in Eq. (11), the PDF depends on the mean as well as the variance. $P(Z_{st})$ is the PDF evaluated at the stoichiometric mixture fraction and the variance at a particular CFD cell.

The species mass fraction at each cell from flamelet l is calculated using Eq. (12)

$$\widetilde{Y}_{l,i}(x,t) = \int_0^1 Y_{l,i}(Z,t)P(Z;x,t)dZ \tag{12}$$

The contribution of flamelet l is obtained using the table lookup given by a 4 dimensional linear interpolation:

$$\tilde{Y}_{l,i} = \widetilde{Y_{l,i}}\left(\widetilde{Z_l}, Z_v, \widehat{\chi_{st}}(l), t_l\right), \tag{13}$$

Species mass fraction at each cell is calculated as the weighted average of contributions from all n flamelets.

$$\tilde{Y}_i = \sum_{l=1}^{n}\frac{Z_l}{Z}\tilde{Y}_{l,i} \tag{14}$$

The schematic of the model's coupling with the CFD code is shown in Fig. 1. At the end of each time-step the scalar dissipation rate of each flamelet and residence time along with mixture fraction and mixture fraction variance at each cell are passed to the multidimensional look-up table. The species mass fraction is then interpolated from the library for each flamelet. This is carried out iteratively for each flamelet and the final species mass fraction is calculated using Eq. (14). The temperature at each cell is then calculated from the species mass fraction and enthalpy. The tabulated model in this work assumes the species mass fractions to be represented by a 4 dimensional manifold of scalar dissipation, time, mixture fraction and mixture fraction variance at each time instant. The underlying assumption is that the history effects are negligible. Some more analysis on this aspect and using time as an independent variable is discussed in Appendix B.

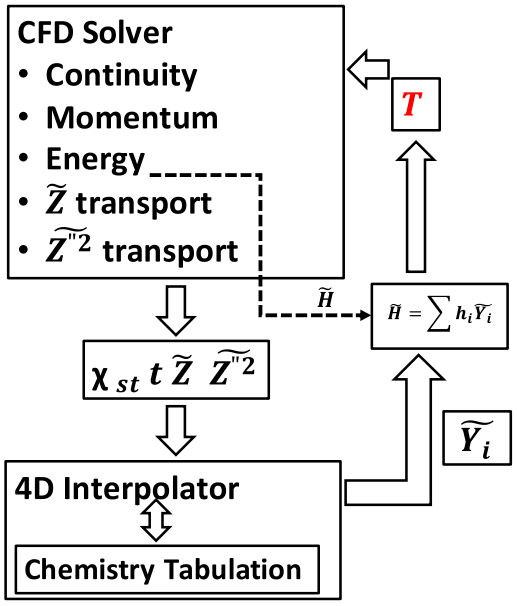

Fig. 1. Schematic of TFM coupling with the CFD code.

Table 1
ECN experimental initial and boundary conditions.

Parameter	Quantity
Fuel	n-dodecane
Nozzle outlet diameter	0.09 mm
Discharge coefficient	0.86
Fuel injection pressure	150 MPa
Fuel temperature	363 K
Injection duration	1.5 ms
Ambient temperature	800-1100 K
Ambient gas density	22.8 kg/m^3
Ambient O_2 concentration	15%

2.4. Computational setup

The TFM combustion approach was initially validated in a LES framework for igniting n-dodecane sprays from the ECN dataset [18] and the condition are shown in Table 1. The experiments consist of an n-dodecane spray injected into a constant volume combustion chamber. The conditions within the chamber can be varied to mimic different operating conditions of diesel engines. In this study, a range of ambient temperatures are considered. The conditions are summarized in Table 1. The baseline condition at 150 MPa injection pressure, 15% Oxygen concentration and 900 K ambient temperature is known as the Spray A condition.

The spray is modeled using a Lagrangian framework and the gas phase is solved using an Eulerian approach. Some experimental and numerical studies [[58],[59]] have focused on the behavior of sprays under engine relevant conditions. In this work the spray breakup and evaporation is modeled as an interfacial system without supercritical behavior. Adaptive mesh refinement is used to refine the grid in regions of high scalar gradients such that the spray and combusting region has a high grid resolution. The spray model has been extensively validated against the ECN dataset for n-dodecane and n-heptane fuels within the LES framework in previous studies by Xue et al. [60]. Grid convergence studies with the dynamic structure LES model [61] suggested a minimum cell size of 0.0625 mm to capture the liquid length and vapor penetration for the n-dodecane sprays. Grid resolution studies for combusting cases with TFM were carried out in the previous study by Ameen et al. [18] and a resolution of 0.0625 mm was shown to capture the relevant physics and was a good compromise between accuracy and wall-clock time. Our previous studies [[38],[39]] also investigated the number the criterion for selecting the total number of flamelets under Spray A conditions. 20 flamelets have been found to be sufficient for the Spray A conditions with injection duration of 1.5 ms. For higher injection durations, the number of flamelets need to be increased proportionately. The chemistry mechanism used to generate the tabulation was derived from the LLNL detailed mechanism with 2755 species and 11,173 reactions [62]. The detailed mechanism was reduced using DRGX (direct relational graphs with expert knowledge) and sensitivity analysis by Luo et al. [63] followed by validation in 0D, 1D and CFD simulations. The details of the spray model and computational setup are summarized in Table 2. Further details and validation studies can be found in our previous publications [12,14,16,18,50] and hence not shown here for brevity.

Table 2
Computational setup.

Modeling Tool	CONVERGE v2.1
Dimensionality and type of grid	3D, with Adaptive Mesh Refinement
Spatial discretization approach	2nd order finite volume
Smallest and largest characteristic grid sizes	Base grid size: 1 mm Finest grid size: 0.0625 mm Gradient based AMR on velocity and temperature fields Fixed embedding in the near nozzle region: 0.0625 mm
Total grid number	22 million at 1 ms
Turbulence and scalar transport models	Dynamic structure LES model
Spray models	Breakup: KH-RT Drag-law: Dynamic model Evaporation model: Frossling correlation
Time step	Variable time step
Combustion models	TFM
Number of flamelets	20
Time discretization scheme	PISO (Pressure Implicit with Splitting of Operators)

3. Results and discussion

Following the detailed description of the modeling approach, this section will focus on the results and discussion. The validation of the TFM approach within the LES framework will be presented first.

3.1. Ambient temperature sweep

Validation of the TFM in an LES framework is shown for different ambient temperature conditions from the ECN. Since the LES spray set-up has already been validated against experimental data for mixture fraction, vapor penetration and liquid length in our previous studies [60], it is not shown here for the sake of brevity. Three LES realizations were carried out for each ambient temperature condition based on previous work from our group [16]. More details about the multiple LES realizations will be discussed in the following paragraphs. The injection pressure, ambient density and oxygen concentration were kept constant across all the cases. Ignition delay is defined as the time required to reach 14% of maximum OH in the computational domain at quasi steady state of the flame. The liftoff length is defined as the distance from the nozzle tip where the OH mass fraction reaches 14% of maximum OH at steady state. These definitions are based on ECN recommendations [64] and consistent with previous studies [14,18]. The ignition delay and liftoff predictions from TFM are compared to experimental measurements in Fig. 2. Each realization is represented with a

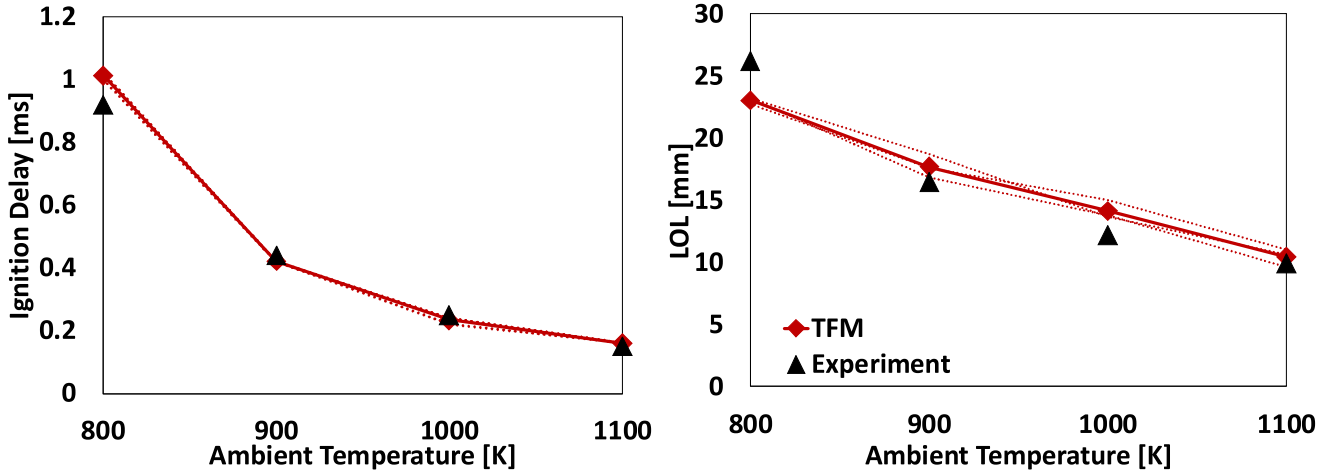

Fig. 2. Ignition delay and liftoff length predicts from TFM for different ambient temperatures. Dotted lines represent each realization and the solid line represents average of the 3 different realizations. Experimental data is obtained from the ECN [64].

dotted line and the solid line represents the average ignition delay from the different realizations. Increase in ambient temperature results in lowering of ignition delay and flame liftoff length, which is expected. This trend is captured well by the simulations. The ignition delays are predicted accurately between 900 to 1100 K range, while 11% over prediction is observed at 800 K. After ignition, the flames reach a quasi-steady state and the liftoff length stabilizes by ~1 ms for 900 K to 1100 K conditions. The 800 K case ignites at the later stage and reaches a quasi-steady state at 1.3 ms. Variations in ignition delay among the 3 different realizations are minimal. The model is also observed to capture the trends in liftoff length accurately with slight over predictions for 900 K and 1000 K condition, and 12% under prediction at 800 K. The variations from one realization to another are more prominent in the liftoff length predictions. A difference of 2 mm is observed at the baseline 900 K case. Each of the realizations are carried out with the 0.0625 mm mesh resolution as mentioned in Table 2. Different flamelet libraries were generated for each ambient temperature condition with the same table resolution that is mentioned in Section 2.2. The table needs to be generated once for each realization. One of the advantages of using a tabulated model is the ability to reuse the library for multiple realizations thus reducing the computational overhead. Each realization was run with 200 processors in parallel at an approximate cost of 20,000 CPU hours per simulation at the 900 K condition. The computation cost varied with the ambient temperature condition.

The different LES realizations were obtained by perturbing a random number seed that influences the droplet initialization and turbulence-spray interaction. During the droplet initialization, the injected parcels are given velocities with a random direction within the spray cone. In the turbulent dispersion model, the velocity of the spray parcels are modified by adding a turbulent velocity based on the turbulence intensity in the computational cell. The random numbers used in both these processes are governed by the random seed prescribed at the start of the simulation. The validity of this method of perturbing the LES solution was investigated by Ameen et al. [16]. Xue et al. [60] previously showed that a single realization is sufficient to capture the global spray parameters. However, capturing local mixing and velocity fields require multiple realizations. Recently, Van Dam et al. [65] have shown that the random number seed is a reasonable approach to perturb the initial conditions of spray injection in the absence of uncertainty measurements from experiments. Pei et al. [14] showed that 5 realizations are required to capture the global combustion trends accurately. Ameen et al. [16] showed that a combination of azimuthal and ensemble averaging can lead to reduced computational costs with lesser number of realizations. Azimuthal averaging for temperature and OH mass fraction fields are performed on 128 planes for each realization, followed by ensemble averaging of the three different realizations. The statistically averaged temperature and OH mass fraction contours are shown in Fig. 3 for different ambient temperatures. The black line represents the iso-line of the stoichiometric mixture fraction. The averaging process is carried out for the time step where the flame reaches a quasi-steady state. At 1 ms for the 900, 1000 and 1100 K cases, higher temperatures show higher jet penetration and narrower spreading angles owing to the early ignition. The formation of OH corresponds with the high temperature flame region. High concentration OH regions are observed at the lateral edges of the jet near stoichiometric regions, away from the spray axis with lower concentration at leading edge for the 1100 K case. This can be attributed to recirculation zones at the edge leading to higher residence time and also lower scalar dissipation rates in these regions. Lower ambient temperatures of 1000 K and 900 K led to more spreading of the jet along with higher liftoff lengths and lower OH concentrations at the leading edge. With further decrease in ambient temperatures and consequently higher ignition delays at 800 K, OH is observed to form away from the stoichiometric region compared to the high temperature cases. Longer ignition delays lead to substantially higher mixing prior to ignition. By the time the low temperature reactions transition to the main ignition, the mixture is much leaner and results in lower peak temperatures and OH concentrations. Overall, the TFM approach is able to capture autoignition and flame liftoff over a range of ECN conditions effectively. Our previous studies [18] also show that the TFM approach is computationally more efficient than the homogeneous reactor model with finite rate chemistry by being at least 50% faster for a given operating condition. Hence, the TFM approach is used to further explore the LTC conditions in the subsequent sections.

3.2. Intermediate species formation

Figure 4 shows a qualitative comparison between the experiments and CFD prediction of CH_2O for a single realization. The CH_2O PLIF images at the baseline Spray A conditions were obtained by Skeen et al. [66] for a single injection. Initial CH_2O formation was observed at the periphery of the penetrating jet followed by convection to the core. This corresponds to the first stage ignition and heat release. In the CFD simulations, the initial formation of CH_2O is observed near the periphery of the jet at approximately

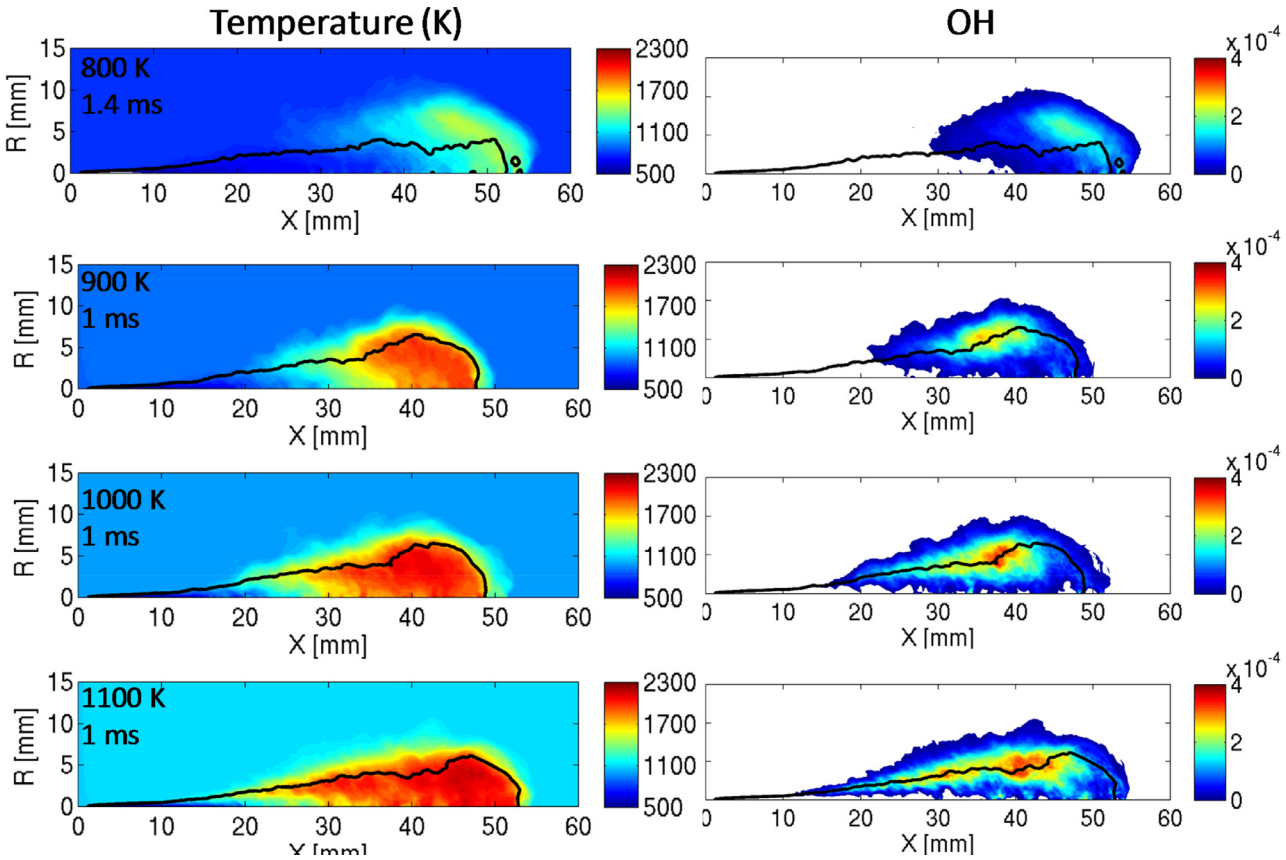

Fig. 3. Temperature and OH mass fraction contours are shown for different ambient temperature conditions at 1 ms for 900 K–1100 K conditions and 1.4 ms for 800 K. Azimuthal averaging is carried out over 128 cut-planes through the spray axis followed by ensemble averaging over 3 LES realizations. (For interpretation of the references to color in this figure legend, the reader is referred to the web version of this article.)

the same location. This is followed by the penetration of the jet with high concentration CH_2O regions forming due to convection along the centerline of the nozzle. The subsequent consumption of CH_2O corresponds to the main ignition event and the high CH_2O concentration region stabilizes at a certain distance from the nozzle. The CFD model is able to predict the same trend. The high concentration region in simulations is predicted a few millimeters downstream as compared to the experiments. This is due to the fact that the model is slightly over-predicting the liftoff lengths at this condition and are also subject to variations in multiple realizations. It must be noted that the experiments were carried out for a single injection event. The resolution in the CFD grid is much higher than the imaging. In order to have a more consistent comparison between experiments and simulations, an ensemble average over multiple injection is preferable. Due to the unavailability of image resolution, the spatial filtering of the LES CH_2O contours was not carried out in this study. Overall, the model is able to capture the qualitative trends gives reasonable predictions for the intermediate species associated with the first stage of ignition.

3.3. Low temperature combustion

Autoignition and flame stabilization of spray flames is a highly coupled problem involving mixing and chemical kinetics. Reduction in ambient temperature can lead to significant changes in the overall process leading to species formation and heat release in a different regime. Modern internal combustion engine design concepts are trying to achieve low temperature combustion in order to reduce pollutant formation. In this part of the study, the validated computational setup shown above is used to investigate and highlight species formation and flame stabilization at an ambient temperature of 750 K. Comparative studies are carried out against the baseline Spray A case at 900 K to understand the fundamental differences at LTC conditions. The duration of injection at this condition is 6 ms compared to the 1.5 ms injection duration for the baseline condition. Ignition is observed at approximately 1.8 ms in the experiments at 750 K. At temperatures above 900 K the spray reaches a quasi-steady state by 1 ms. This clearly shows a significant difference in the time and length scales involved under LTC conditions. Longer injection durations and simulation times imply larger jet and flame penetrations, thus requiring a much larger computational domain and number of cells. This increases the computational cost and memory requirements nonlinearly. A single LES realization was carried out using the TFM approach for the LTC condition. The same chemistry mechanism with 103 species and 370 reactions was used to generate the flamelet libraries. The injection pressure was set at 150 MPa with an ambient chamber density of 22.8 kg/m^3, 15% O2 and 750 K ambient temperature. The simulation was run up to 3.56 ms of injection, by this time the species profiles and flame liftoff are observed to reach a quasi-steady state. The computational cost was approximately 55,000 CPU hours with this setup.

Previous DNS studies by Chan et al. [67] investigated the effect of the terms in the flamelet equation tangential to the stoichiometric surface. These terms were lumped together and found to be negligible for diffusion flame configurations. Such DNS studies are not feasible at this point for the current LTC case owing to the higher Reynolds numbers, injection durations and pressures. However, the terms are heavily dominated by spatial gradients in mixture fraction (∇Z) and species mass fraction (∇Y_i). For these LTC cases at 750 K, during ignition, the mixture is significantly homogeneous compared to the high temperature cases. These terms will

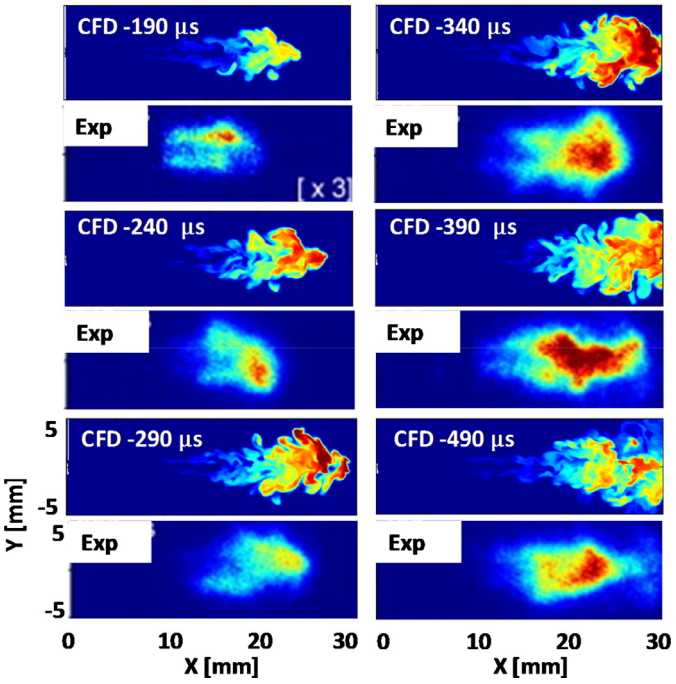

Fig. 4. False color images of formaldehyde PLIF for a single injection at Spray A conditions [66] (bottom) are compared with the CFD predictions (top) from a single realization.

tend to 0 and hence the contribution will be very low. Moreover, the unsteady flamelet model with multiple flamelets for a small χ reduces to $\frac{\partial Y_i}{\partial t} = \dot{\omega}_i$; which makes the model similar to a multi-zone model where chemistry is discretized over a range of mixture fractions. This was also pointed out by Hergart et al. [68]. As a result, the unsteady flamelet model has been used in many previous studies to model non-premixed flames characterized by ignition at homogeneous and partially premixed conditions. A list of validation and previous work is listed in Refs. [47–49,68–70]. Recently, Dahms et al. [7] employed chemical explosive mode analysis and showed that the flamelet assumption is valid during the entire ignition event for ECN Spray A. As a result, the current formulation can be used to model the LTC regime.

3.3.1. Jet penetration

Since the 750 K condition has not been simulated with LES in the past, spray validation is presented first. The jet penetration is calculated from the mixture fraction fields and compared with the experimental data available from the Schlieren imaging in Fig. 5. It is defined as the maximum axial distance of the 0.1% mixture fraction contour from the injector for the CFD simulations as per the recommendation from ECN [64]. The single LES realization is able to capture the jet penetration accurately. Some over prediction is observed in the initial part of the injection, i.e., from 0.2 ms to 0.5 ms. Mixing predictions are important as they determine the equivalence ratio of the combusting mixture and the resulting temperatures and species formation.

3.3.2. Ignition delay and flame liftoff

Spray flames established with higher hydrocarbons (C7 and above) are typically characterized by two stage ignition. The low temperature formation reactions lead to an initial heat release followed by the main ignition event. Experimental studies [66] have shown that formaldehyde (CH_2O) is an important intermediate species and its formation corresponds to the first stage ignition. The maximum CH_2O and OH in the domain are plotted vs. time in Fig. 6. For the 750 K case, formaldehyde formation is observed

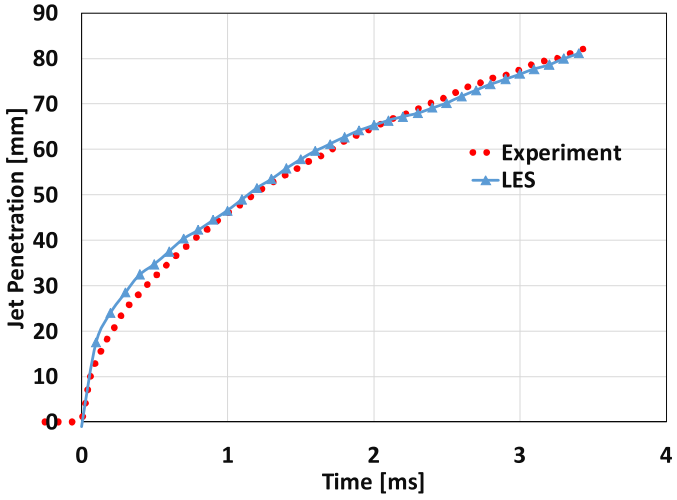

Fig. 5. Jet penetration at 750 K ambient temperature compared with experimental measurements from ECN [64].

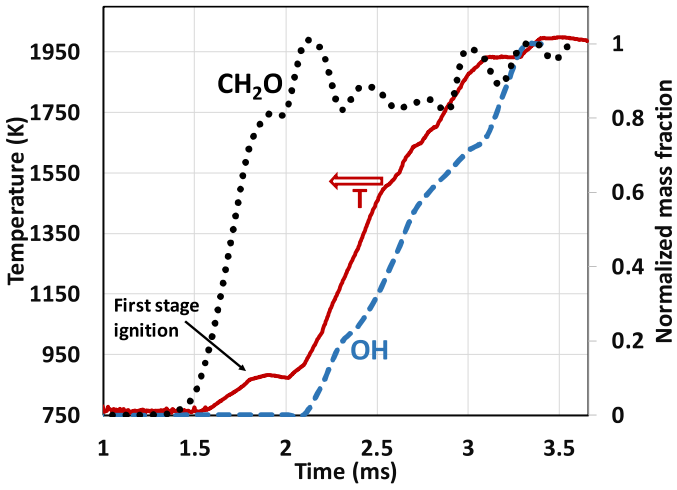

Fig. 6. Predicted formaldehyde (line) and OH (dots) formation at 750 K vs. time.

to begin at 1.5 ms which also corresponds to the first stage ignition. The concentration of formaldehyde increases sharply and then reaches a quasi-steady state. The consumption of CH_2O is followed by the formation of OH at 2.1 ms which corresponds to the main ignition. The flame reaches a statistically steady behavior by 3.3 ms.

CH_2O, OH and temperature contour plots at a plane passing through the spray axis for different times are shown in Fig. 7. CH_2O formation is first observed approximately 30 mm from the nozzle at 1.5 ms followed by a high concentration region developing along the centerline corresponding to the formation of a cool flame at 2 ms. This is followed by the consumption of CH_2O and these regions correspond to high OH concentration and high temperature flame spots at 3 ms. The high temperature regions are observed to form in the outer periphery of the jet where the residence times are highest. The flame is observed to stabilize near the experimentally measured liftoff location represented by the vertical line.

The temporal evolution of liftoff length compared to experiments is shown in Fig. 8. The ignition delay is predicted from the simulations is 2.3 ms. The experimental data set from Sandia for this condition consists of two experiments with two different injectors with the same nominal diameters. The experimental ignition delay for Injector 1 is reported as 1.79 ms and 2.5 ms for In-

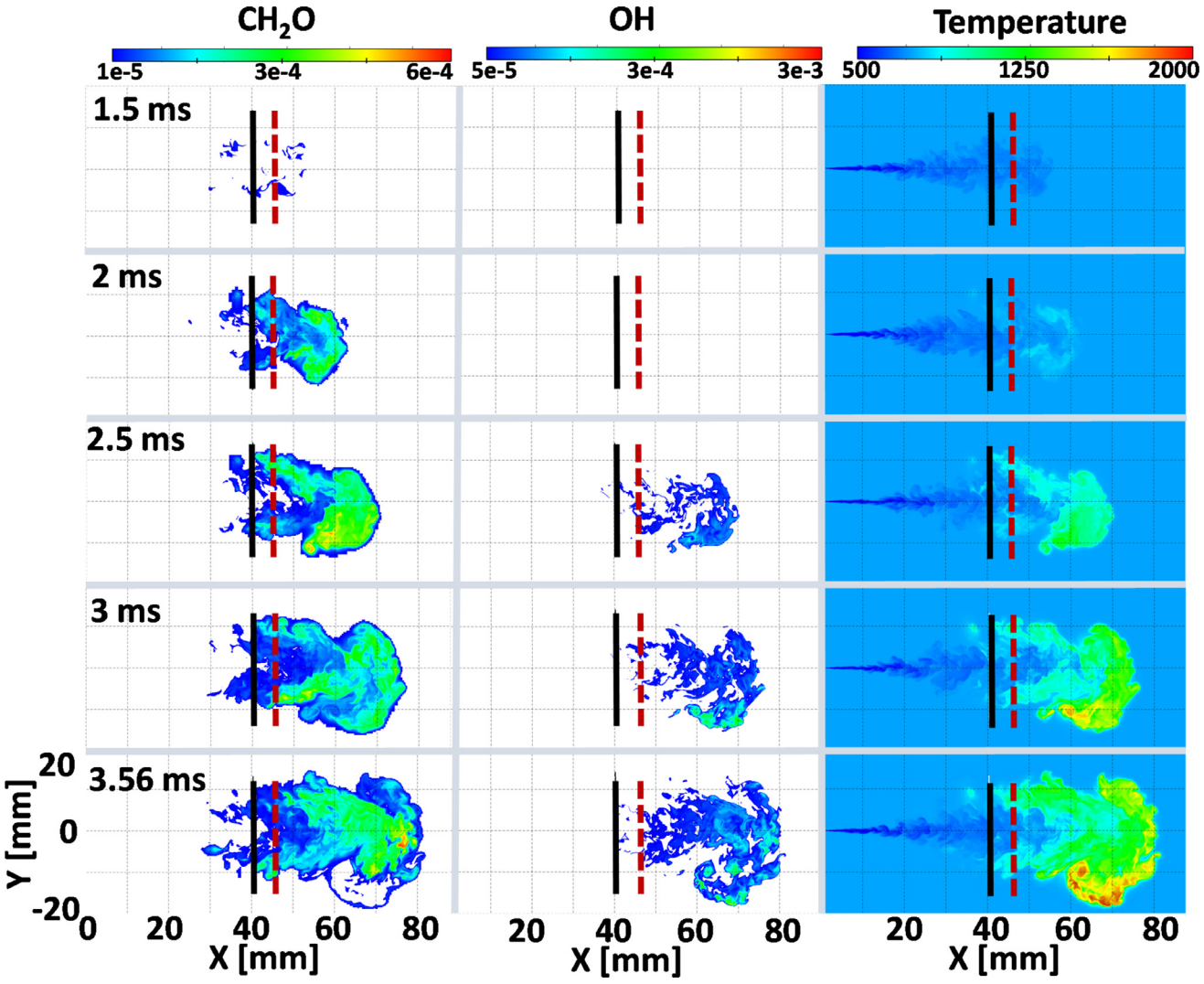

Fig. 7. Temporal evolution of CH_2O, OH mass fraction and temperature contours at 750 K predicted by TFM. The vertical solid line represents the measured liftoff length from experiments using Injector1 and the dashed line represents the measured liftoff length from Injector 2. (For interpretation of the references to color in this figure legend, the reader is referred to the web version of this article.)

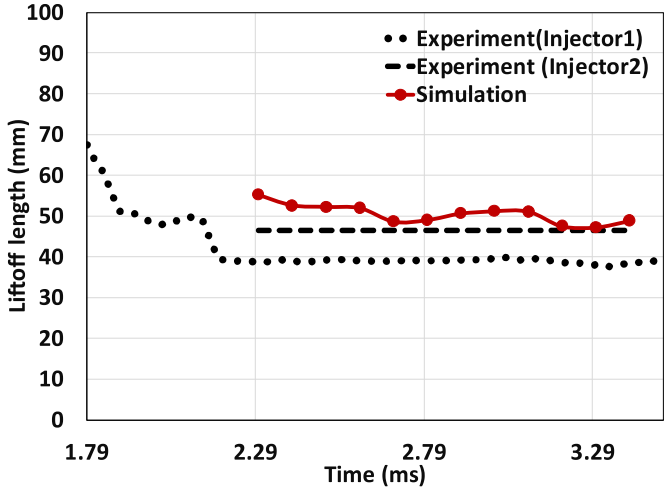

Fig. 8. Liftoff length vs. time at 750 K from simulation compared with the experimental data from ECN.

jector 2 at this condition. The simulation is able to capture the ignition delay and flame liftoff close to the predictions from the experiments. Under these low temperature conditions, the experimental uncertainty is relatively high [71]. Higher fidelity chemistry mechanisms (perhaps a detailed mechanism) can capture the LTC ignition and flame liftoff length more accurately. This motivates us to perform future simulations with detailed mechanism and TFM under the LTC condition.

3.4. Differences between low and high temperature combustion

The ignition delays and flame liftoff lengths increase substantially as the ambient temperature is reduced from 900 K to 750 K. This part of the study investigates the differences at these two conditions using qualitative and quantitative results. Translucent OH iso-volumes are rendered for the two conditions at a time instant after ignition; 0.6 ms for 900 K and 3 ms for 750 K and shown in Fig. 9. It is important to note that ignition happens at 0.44 ms for 900 K and 2.1 ms for 750 K from simulations. The OH iso-volume is colored by temperature and is superimposed with opaque CH_2O iso-volumes (blue) which span a range of 10^{-3} to maximum mass fraction in the domain. The sequential formation of CH_2O, OH and spatial distribution can be observed for both the conditions. At 900 K, CH_2O formation is observed at an axial distance of 15 mm along the circumference of the spray. This region extends into the core of the flame. OH formation is observed surrounding these iso-

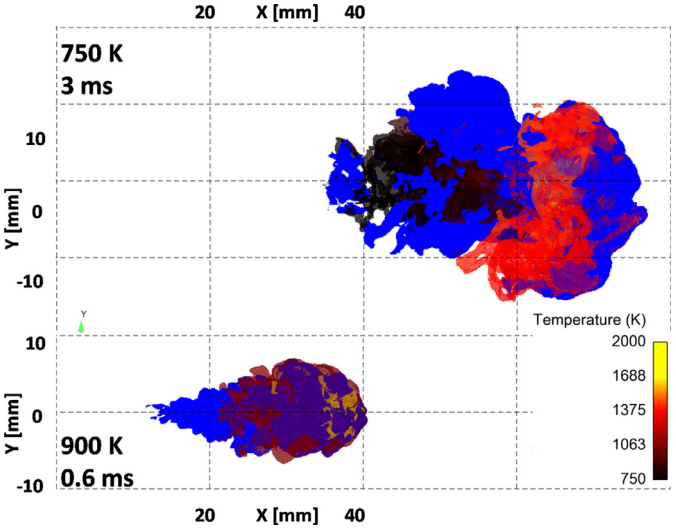

Fig. 9. Flame structure after ignition for 750 K and 900 K ambient temperature conditions. Spatial distribution of CH_2O is represented using opaque blue iso-volumes. OH iso-volumes are colored by temperature. (For interpretation of the references to color in this figure legend, the reader is referred to the web version of this article.)

surfaces corresponding to the consumption of CH_2O. The high temperature regions are observed after the complete consumption of CH_2O. At 750 K, CH_2O formation is significantly downstream of the injector with a much wider distribution in the radial direction. This leads to significantly leaner mixture formation and lower temperatures.

In order to get an overview of the species formation, the reacting field is analyzed in the mixture fraction space. Figure 10 shows the scatter plot of temperature (blue dots) on primary Y-axis and CH_2O on secondary (red dots) Y-axis against mixture fraction for both the temperature conditions at different times. The physical time is normalized (t^*) based on the ignition delay. The vertical line shows the stoichiometric mixture fraction demarcating the lean and rich regions. At 900 K condition (top image in Fig. 9), CH_2O formation and initial temperature rise is observed in the rich region at 0.3 ms i.e., $t^* = 0.68$. The high temperature regions are then observed to move towards the stoichiometric region as they ignite while the CH_2O formation is still in the rich region of the flame. This is in tune with the previous findings from DNS studies. The CH_2O formation peaks at a mixture fraction of 0.15 which corresponds to an equivalence ratio of 3.74. As the fuel is injected into the domain it evaporates and mixes with the ambient oxidizer as time progresses. CH_2O is formed early when the mixture is rich. This is followed by the consumption of intermediate species and formation of high temperature spots in the stoichiometric region. At 1 ms ($t^* = 2.27$), the high temperature region peak stabilizes near the stoichiometric region as observed for a typical diffusion flame.

At the 750 K condition (bottom image in Fig. 9), CH_2O formation is observed primarily in the lean region ($Z < Z_{st}$). The initial temperature rise is also observed in the very lean region followed by the peak moving slightly towards the stoichiometric regions. As the ignition delay at 750 K is very high, the time required for the formation of intermediate species is also very high. Higher residence times lead to a significantly leaner mixture. As a result, most of the reactions are in the lean region leading to lower mass fraction and significantly lower temperatures. This is a key difference between the low and high temperature conditions as predicted by the simulations.

Figure 11 compares the equivalence ratio – temperature plots for the 750 K and 900 K conditions. It can be observed that the 750 K condition has significantly lower temperatures and equivalence ratios. The LTC conditions show the possibility of soot free combustion as the peak equivalence ratios in the high temperature region are less than 1. This mode of combustion where equivalence ratios are less than 2, has been referred to as Lean Lifted Flame Combustion and has the potential to eliminate soot [1,72]. At 900 K, low temperature heat release is observed to begin at equivalence ratios of 4 whereas at 750 K the heat release is observed when the mixture reaches an equivalence ratio of approximately 1.

3.5. Role of turbulence chemistry interaction

Scalar dissipation at the sub grid scale is known to play an important role in autoignition and flame stabilization mechanism

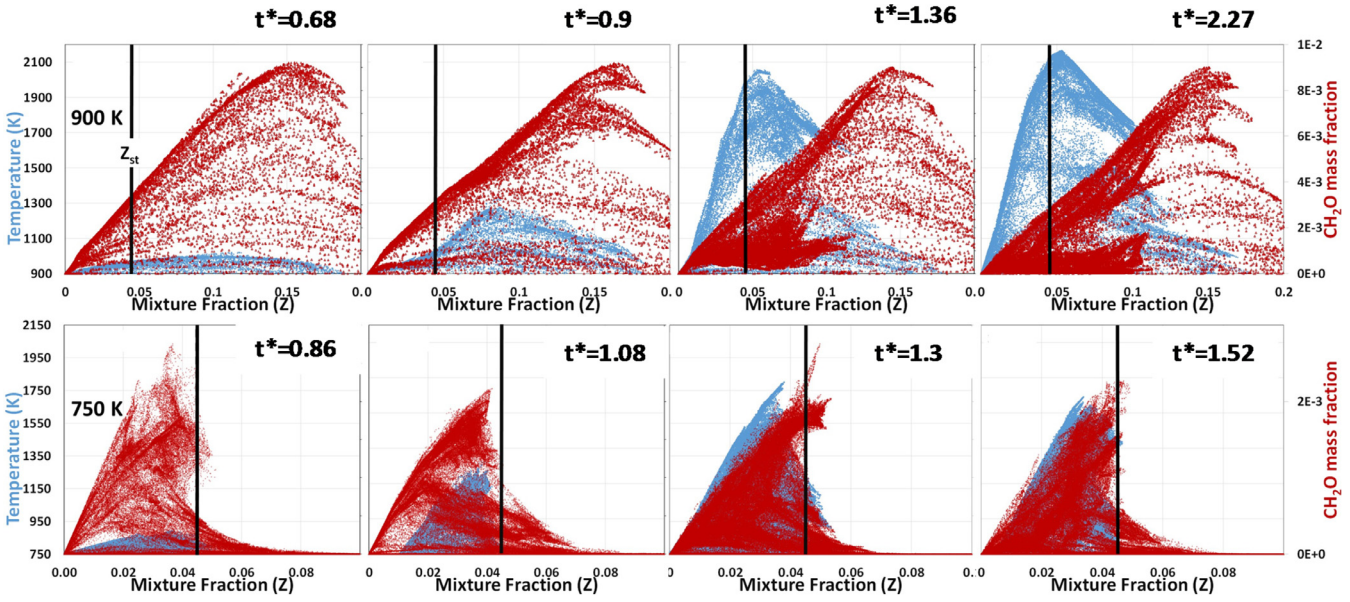

Fig. 10. CH_2O mass fraction (red dots) and temperature (blue dots) evolution in mixture fraction space at 900 K (top) and 750 K (bottom) ambient temperature conditions. The time (t^*) has been normalized based on the ignition delay for the 900 K and 750 K ambient temperature. (For interpretation of the references to color in this figure legend, the reader is referred to the web version of this article.)

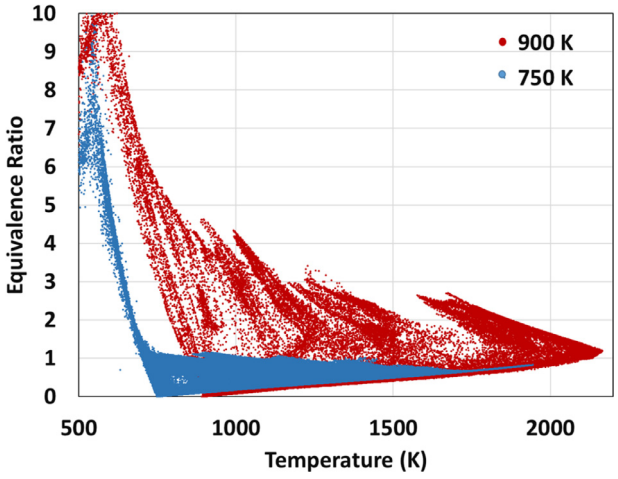

Fig. 11. Equivalence ratio-temperature scatter plots for 900 K at 1 ms (red) and 750 K at 3.5 ms (blue) conditions. (For interpretation of the references to color in this figure, the reader is referred to the web version of this article.).

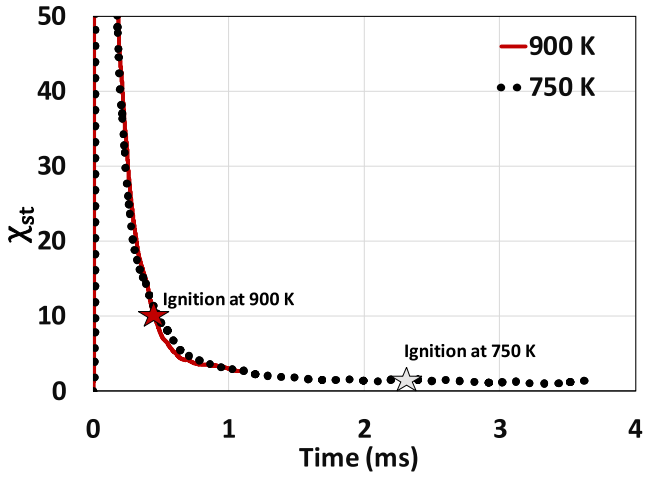

Fig. 12. Temporal evolution of scalar dissipation rate at 900 K and 750 K for first flamelet.

[4–6]. Higher values of scalar dissipation lead to lower temperatures and ignition delays. At sufficiently higher values of χ_{st} the flame extinguishes. It was observed that the simulations with a homogeneous reactor assumption fail to predict ignition at the 750 K condition. It must be noted that most of the flame stabilization region for these LTC conditions are significantly downstream of the liquid spray. As a result, the scalar dissipation experienced at the autoignition and flame stabilization locations are significantly lower compared to the high temperature cases. The stoichiometric scalar dissipation rate for the 1st flamelet is plotted vs. time for the two temperature conditions in Fig. 12. The scalar dissipation rate increases sharply at start of injection and then decays as the stoichiometric regions move away from the liquid spray. The ignition at 750 K case is characterized by significantly lower and steady scalar dissipation rates compared to the 900 K case. Previous work by the authors [50] showed that as $\frac{d\chi st}{dt}$ approaches 0, the unsteady effects are small.

This part of the study investigates the role of scalar dissipation in the ignition process. 1D flamelet equations are solved with the same set of boundary conditions (as in the CFD simulations), i.e., 22.8 kg/m^3 ambient density, 750 K oxidizer temperature and 15% O_2 oxidizer composition with the 103 species n-dodecane mechanism. In the first case, the stoichiometric scalar dissipation rate (χ_{st}) is set equal to 0. This represents a homogeneous reactor. In the second case, a very small value of scalar dissipation (2 s^{-1}) is added. Note that $\chi_{st} = 2$ s^{-1} corresponds to the scalar dissipation rate at ignition for the 750 K case (refer to Fig. 11). Temperature is plotted vs. mixture fraction in the lean region (clipped up to

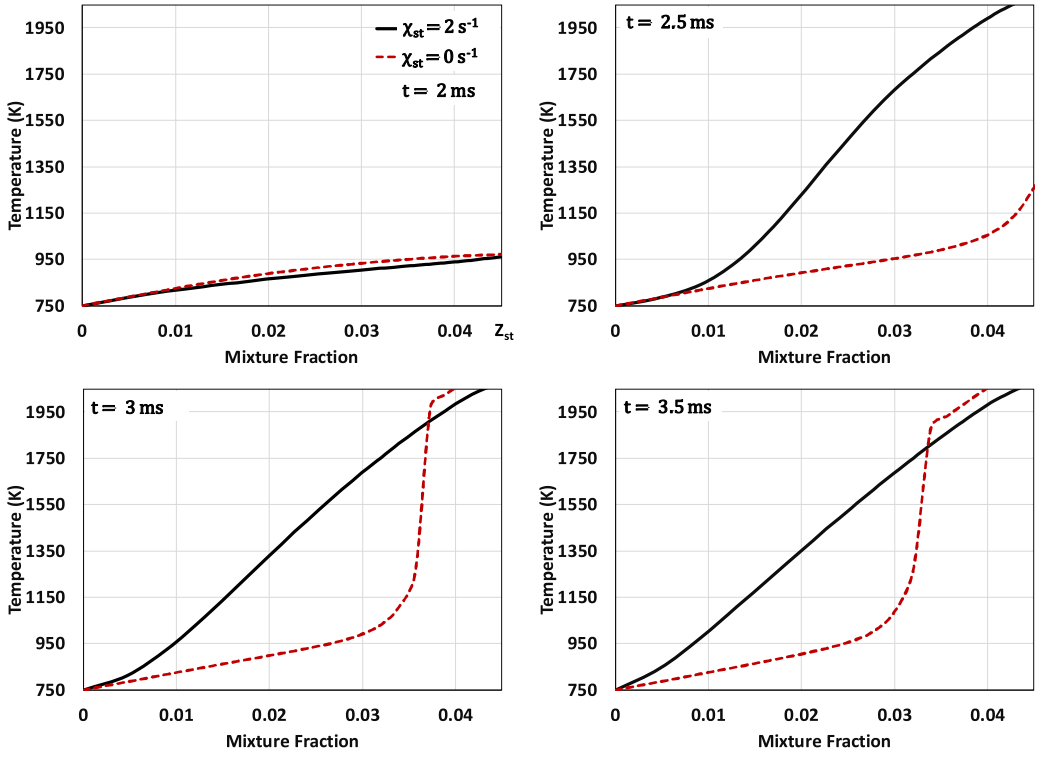

Fig. 13. Ignition of flamelets at 750 K for 2 conditions: (i) Stoichiometric scalar dissipation rate = 2 s^{-1} (solid line) (ii) homogeneous reactor assupmtion (dashed).

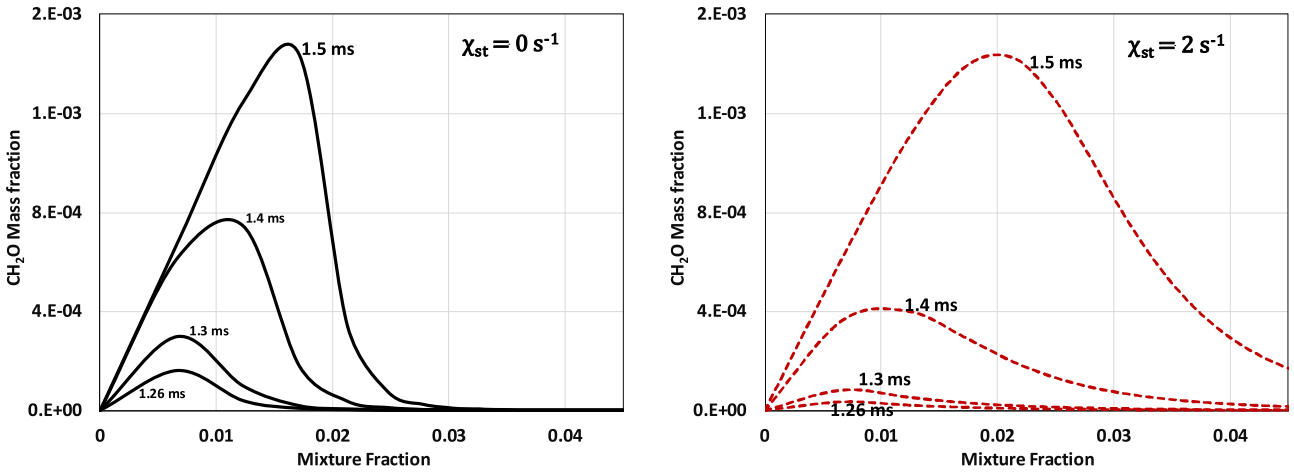

Fig. 14. CH_2O formation in mixture fraction space plotted for (i) homogeneous reactor case on left (i.e., 0 s^{-1}) and (ii) flamelet with stoichiometric scalar dissipation rate of 2 s^{-1}. The species profiles with scalar dissipation get broadened in the Z space due to diffusion leading to higher concentration of radicals and intermediate products in the near stoichiometric regions.

$Z = Z_{st}$) in Fig. 13. The first stage of ignition and temperature rise is observed at 2 ms and both models capture this event. The scalar dissipation rate term in the flamelet equation (1) represents the diffusion of radicals in the mixture fraction space. This enhances the ignition at such low temperature conditions. This term is absent for the homogeneous reactor case. The homogeneous reactor case shows significantly delayed ignition in the lean regions as seen from the 2.5 to 3.5 ms duration. The first term on the right hand side of the flamelet equation (1) is the diffusion term and the second term is the species source term. The net species change over a time step is a result of competition between these two terms. Very high scalar dissipation rates lead to an increase in diffusion in the Z space and can lead to extinction of the flamelet. However, at low temperature and low dissipation rates, it is observed that this diffusion can lead to enhancement of the ignition process.

Figure 14 shows the temporal evolution of CH_2O as a function of mixture fraction in the lean region for homogeneous reactor (left) and 2 s^{-1} scalar dissipation rate (right) cases. In both cases, formation of CH_2O is observed at mixture fractions lower than 0.01 and this peak then moves towards the stoichiometric mixture fraction as time progresses. The homogeneous reactor case is characterized by higher CH_2O concentrations. At the corresponding time step with a scalar dissipation rate (Fig. 14 right) shows a diffused profile with lower peak values. As a result of diffusion, the radicals and intermediate species near the stoichiometric regions reach a higher value compared to the homogeneous reactor case. This enhances the ignition process and leads to the main ignition event which then propagates into the lean regions. It is observed that in absence of this diffusion i.e., the homogeneous reactor case, the main ignition does not take place in the lean regions. As a result, the homogeneous reactor case cannot predict any ignition for the spray flame at the 750 K condition. Scalar dissipation plays an important role in enhancing the ignition process and computational models need to account for such TCI effects.

4. Summary and conclusions

A recently developed Tabulated Flamelet Model was implemented for performing multiple LES realizations of spray flames. The ECN spray conditions for n-dodecane fuel were initially simulated for the temperature range of 800 K to 1100 K. A mesh of 0.0625 mm minimum cell size and approximately 22 million cell count was used for each LES realization. The ignition delays did not differ significantly between the realizations, however, variations in flame liftoff length were observed between these realizations. Azimuthal and ensemble averaging between different realizations were carried out for temperature and OH mass fraction. These results were used to study the structure of the flame for different temperature conditions. Overall, the tabulation approach is able to capture the igniting spray conditions over a range of temperatures when compared with ECN data. This model setup was used to study the autoignition and flame stabilization at 750 K ambient temperature condition. This condition is characterized by larger injection duration and ignition delay compared to the baseline 900 K condition, which increased the computational cost drastically. LES performed at this condition was used to understand autoignition and flame stabilization mechanisms and how they differ from tradition high temperature mixing controlled combustion. At the 750 K condition, the jet penetration is captured accurately up to the simulated time of 3.5 ms. CH_2O formation was observed to begin at 1.5 ms followed by ignition at 2.3 ms in the simulations. The flame liftoff length and ignition delay were over predicted by the TFM approach while the homogenous reactor model could not predict ignition under these conditions. Qualitative results were presented to show the spatial and temporal distribution of intermediate and high temperature species under 750 K and 900 K condition. Some of the major differences with respect to the baseline 900 K case can be summarized as follows:

1. Formaldehyde formation is observed in lean regions (phi < 1) for the 750 K case compared to rich regions at 900 K.
2. At ambient temperatures of 900 K, CH_2O formation is observed in the rich regions followed by OH and high temperature in the stoichiometric regions. Higher ignition delay at 750 K leads to significantly leaner mixture formation, leading to significantly lower mass fractions of CH_2O, OH and flame temperatures. The phi-T plots show a leaner combustion with equivalence ratios below 1 for the 750 K case. This could possibly lead to soot free combustion.
3. The ignition at 900 K occurs at relatively higher scalar dissipation rates compared to 750 K.

Scalar dissipation is observed to play an important role in enhancing ignition at these low temperature conditions characterized by two stage ignition. Comparative studies with homogeneous reactor simulations were presented. The first stage ignition and temperature rise is not influenced by turbulence. However, scalar dissipation causes these low temperature radicals and intermediate species to diffuse towards the relatively richer regions. Under these conditions, it is observed that the diffusion process plays a pivotal

role in the main ignition. It not only accelerates the main ignition process, but the flame fails to ignite in absence of this diffusion process at the 750 K condition. Similar reduction of the main ignition delay due to dissipation was also reported by Krisman et al. [6] in their 2D DNS studies under lower pressure and richer conditions. The results show that the TFM model coupled with LES is able to capture the ignition delay and liftoff across a wide range of temperature conditions and provide new insights into the combustion process, especially under LTC conditions.

Acknowledgment

The submitted manuscript has been created by UChicago Argonne, LLC, Operator of Argonne National Laboratory (Argonne). Argonne, a U.S. Department of Energy Office of Science laboratory, is operated under Contract No. DE-AC02-06CH11357. The U.S. Government retains for itself, and others acting on its behalf, a paid-up nonexclusive, irrevocable worldwide license in said article to reproduce, prepare derivative works, distribute copies to the public, and perform publicly and display publicly, by or on behalf of the Government. The research was funded by DOEs Office of Vehicle Technologies, Office of Energy Efficiency and Renewable Energy under Contract No. DE-AC02-06CH11357. The authors are grateful to Lyle Pickett and Scott Skeen from Sandia National Laboratory for providing the CH_2O PLIF data. The authors would also like to thank Umesh Unnikrishnan for help with the flamelet code. The authors wish to acknowledge the computational resources of 'Fusion' and 'Blues' clusters at Argonne National Laboratory.

Appendix A. Real gas effects on the flame development

In the current study, the ideal gas equation of state (EOS) was used to solve the flamelet equations and generate the tabulated profiles used in the TFM model. Using the ideal gas assumption implies that the compressibility factor, Z ($=pv/RT$) is assumed to be unity. While conditions of the combustion products are sufficiently far separated from the critical point, these flow-conditions exhibit appreciable compressibility so that $Z=1$ can predict incorrect density and with this the overall rate of fuel conversion. In this section, the validity of using the ideal gas assumption is evaluated by incorporating the more accurate Peng–Robinson EOS to the flamelet equation, and comparing the solutions of these equations to those using the ideal gas EOS. The Peng–Robinson EOS is given by

$$p = \frac{RT}{v - b_m} - \frac{a_m}{v^2 + 2b_m v - b_m^2} \tag{A1}$$

Here, p is the pressure, T is the temperature, v is the molar volume, R is the universal gas constant, and a_m and b_m are parameters which depend on the critical temperature, critical pressure and the acentric factor of the mixture. Using this equation leads to a cubic equation for the compressibility factor ($Z=pv/(RT)$) and thus Peng–Robinson EOS is called as a cubic equation of state. Miller et al. (Miller, R., Harstad, K., & Bellan, J. (2001), "Direct numerical simulations of supercritical fluid mixing layers applied to heptane–nitrogen", *Journal of Fluid Mechanics*, 436, 1-39) discusses methods of evaluating these parameters for a multi-component gas mixture. The value of the binary interaction parameter is available only for a limited pairs of species, and hence it is assumed here that the binary interaction parameter between any two species is assumed to be 0. With this assumption, the parameters a_m and b_m are given by:

$$a_m = 0.457236\frac{(RT_{cm})^2}{P_{cm}}\left[1 + c_m\left(1 - \sqrt{\frac{T}{T_{cm}}}\right)\right]^2 \tag{A2}$$

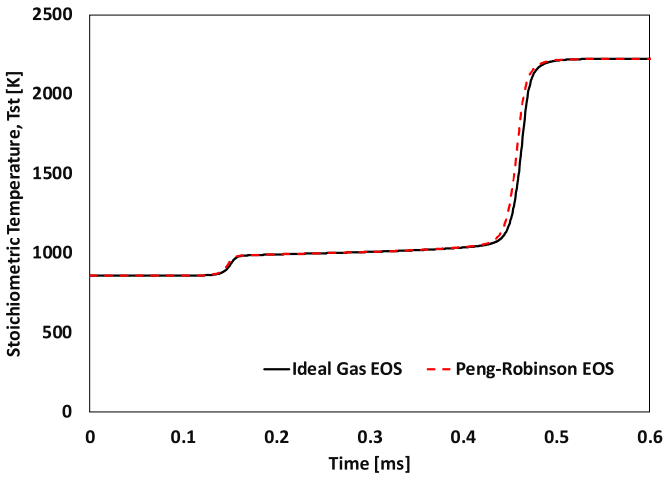

Fig. A1. Evolution of the stoichiometric temperature of the flamelet with time for $\chi_{st} = 1\ s^{-1}$ using the ideal gas and Peng–Robinson EOS.

$$b_m = 0.077796\frac{RT_{cm}}{P_{cm}} \tag{A3}$$

where, c_m is given by

$$c_m = 0.37464 + 1.54226\omega_m - 0.26992\omega_m^2 \tag{A4}$$

In Eqs. (A2)–(A4), T_{cm}, P_{cm}, and ω_m are the pseudo-critical temperature, pressure, and acentric factor, respectively, which depend on the molar composition of the mixture. These pseudo-critical parameters are obtained as:

$$T_{cm} \approx \frac{\left[\sum_i x_i \frac{T_{ci}}{\sqrt{P_{ci}}}\right]^2}{\sum_i x_i \frac{T_{ci}}{P_{ci}}} \tag{A5}$$

$$P_{cm} = \frac{T_{cm}}{\sum_i x_i \frac{T_{ci}}{P_{ci}}} \tag{A6}$$

$$\omega_m = \sum_i x_i \omega_i \tag{A7}$$

Here, x_i is the mole fraction of species i, and T_{ci}, P_{ci}, and ω_i are the critical temperature, pressure and acentric factor of species i respectively. The critical temperature, pressure and acentric factors are available only for the major species. So, in this section, only 5 species – nC12H26, O2, N2, H2O and CO2 – are used to determine the critical parameters in Eqs. (A5)–(A7).

To ensure self-consistency, all the thermodynamic properties of the mixture are also evaluated using the Peng–Robinson EOS. The molar enthalpy, h, and the molar heat capacity at constant pressure, c_p, are given by

$$h = h^0 + pv - RT + K_1\left(a_m - T\frac{\partial a_m}{\partial T}\right) \tag{A8}$$

$$c_p = c_p^0 - T\frac{\left(\frac{\partial p}{\partial T}\right)_{v,X}^2}{\left(\frac{\partial p}{\partial v}\right)_{T,X}} - R - T\frac{\partial^2 a_m}{\partial T^2}K_1 \tag{A9}$$

Here, h^0 and c_p^0 are the reference molar enthalpy and the reference molar heat capacity respectively, which are obtained from Chemkin libraries (which make the ideal gas EOS assumption). The additional parameters in Eqs. (A8) and (A9) are related to the pseudo-critical parameters as shown in Eqs. (A10)–(A14).

$$K_1 = \frac{1}{2\sqrt{2}b_m} ln\left[\frac{v + \left(1 - \sqrt{2}\right)b_m}{v + \left(1 + \sqrt{2}\right)b_m}\right] \tag{A10}$$

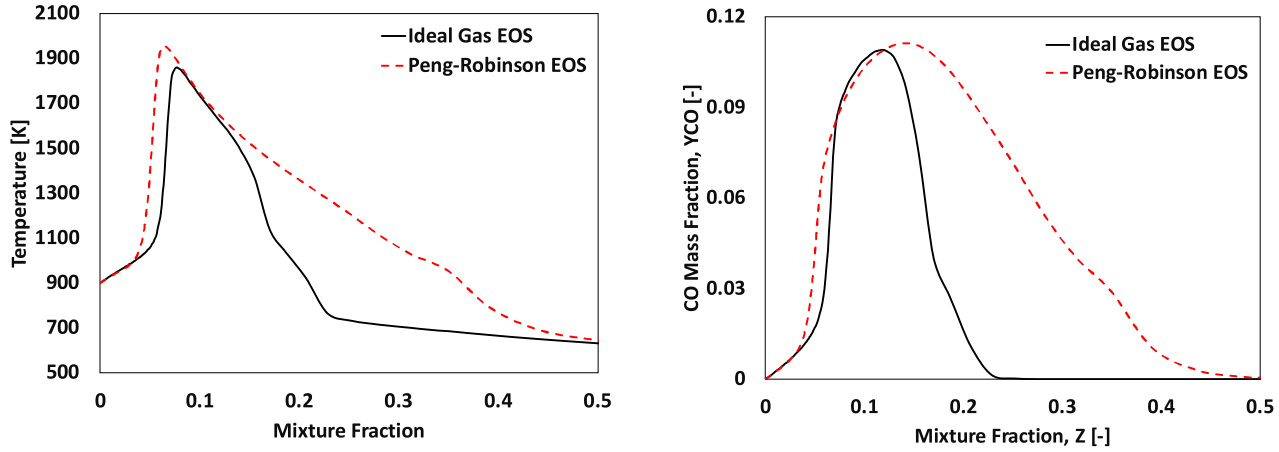

Fig. A2. Profiles of (left) Temperature and (right) CO mass fraction in the mixture fraction space at a time of 0.4 ms. The profiles are obtained by solving the flamelet equation with $\chi_{st} = 1\ s^{-1}$.

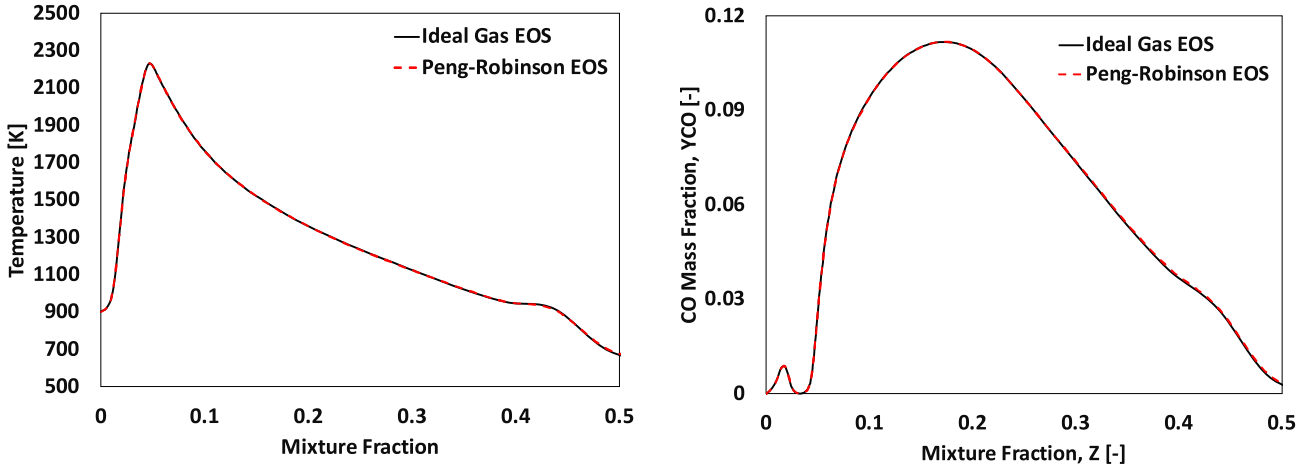

Fig. A3. Profiles of (left) Temperature and (right) CO mass fraction in the mixture fraction space at a time of 1.0 ms. The profiles are obtained by solving the flamelet equation with $\chi_{st} = 1\ s^{-1}$.

$$\frac{\partial a_m}{\partial T} = -\frac{a_m c_m \sqrt{\frac{T}{T_{cm}}}}{T\left(1 + c_m\left(1 - \sqrt{\frac{T}{T_{cm}}}\right)\right)} \tag{A11}$$

$$\frac{\partial^2 a_m}{\partial T^2} = \frac{0.457236R^2}{2T} c_m(1 + c_m)\frac{T_{cm}}{P_{cm}}\sqrt{\frac{T_{cm}}{T}} \tag{A12}$$

$$\left(\frac{\partial p}{\partial T}\right)_{v,X} = \frac{R}{v - b_m} - \frac{\left(\frac{\partial a_m}{\partial T}\right)}{v^2 + 2vb_m - b_m^2} \tag{A13}$$

$$\left(\frac{\partial p}{\partial v}\right)_{T,X} = \frac{-RT}{(v - b_m)^2} \times \left[1 - 2a_m\left\{RT(v + b_m)\left(\frac{v}{v - b_m} + \frac{b_m}{v + b_m}\right)^2\right\}^{-1}\right] \tag{A14}$$

The flamelet equations (1) and (2) are solved for a stoichiometric scalar dissipation rate, $\chi_{st} = 1\ s^{-1}$, using both the ideal gas and Peng–Robinson EOS. The boundary conditions correspond to the Spray A baseline case in which the temperature of the oxidizer is 900 K. Figure A1 compares the transient evolution of the stoichiometric temperature for these two cases. It is seen that there is an excellent agreement between the two equations of state. The Peng–Robinson EOS leads to sub-unity compressibility factor estimations, leading to larger density than the ideal gas EOS. This leads to a slightly earlier ignition using the Peng–Robinson EOS as compared to the ideal gas EOS.

Figures A2 and A3 compares the profile of temperature and CO mass fraction in the mixture fraction space using the two approaches. Figure A2 shows that there are marked differences in the flame structure between the two approaches at earlier times. However, Fig. A3 shows that, at steady state, there are negligible differences between the flame structure predictions. The flamelet solution employing the ideal gas EOS ignites slightly later, and thus lags behind the solution employing the PR EOS. Overall, it can be concluded that employing the ideal gas EOS leads to a slightly delayed ignition, but the steady-state flame structure is accurately predicted.

Appendix B

In this work the 4-D flamelet libraries are generated with time as an independent variable. This method leads to some assumptions. This modeling aspect has been discussed in depth previously in the earlier publication [50]. A set of 1D unsteady calculations were performed by imposing a temporally changing scalar dissipation rate over the flamelet. Three scenarios are compared. The first solution was obtained using the traditional unsteady flamelet

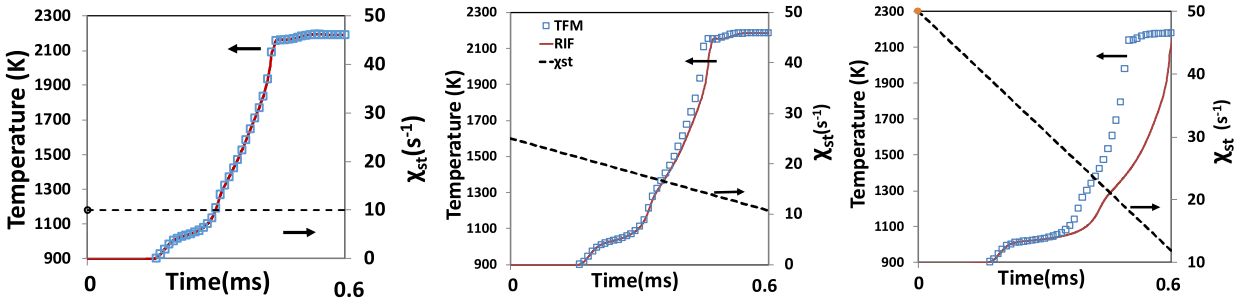

Fig. B1. Maximum temperature vs. time for a flamelet with (i) steady χ_{st} (ii) unsteady χ_{st} with small gradient (iii) unsteady χ_{st} with large gradient.

solver i.e., RIF approach. The same 1D problem is then solved with the TFM approach i.e., the solution Y_i at each point is a function of time, scalar dissipation and mixture fraction. The results are shown in Fig. B1 where the maximum temperature of the flamelet is plotted against time. For case (1), χ_{st} remains steady, case (2) χ_{st} decreases with a small gradient and in case (3) it reduces with a much steeper gradient. As also observed in the previous publication, there are certain differences that are incurred by the use of time as an independent variable as it neglects the history effect. There are no differences for the steady case. As the gradient increases, the history effects become more important. We observe that below a certain gradient (case 2) this difference is small. For the low temperature conditions, which is the main focus of this paper. Figure 11 shows the scalar dissipation rate and it reaches a quasi-steady state with very low gradients. Hence, the impact of this assumption will be small.

References

[1] L.M. Pickett, D.L. Siebers, Non-sooting, low flame temperature mixing-controlled DI diesel combustion, Report No. 2004-010-1399. SAE Technical Paper 2004.

[2] G. Bansal, H.G. Im, Autoignition and front propagation in low temperature combustion engine environments, Combust. Flame 158 (2011) 2105–2112.

[3] S. Mukhopadhyay, J. Abraham, Influence of compositional stratification on autoignition in n-heptane/air mixtures, Combust. Flame 158 (2011) 1064–1075.

[4] S. Mukhopadhyay, J. Abraham, Influence of heat release and turbulence on scalar dissipation rate in autoigniting n-heptane/air mixtures, Combust. Flame 159 (2012) 2883–2895.

[5] G. Borghesi, E. Mastorakos, R.S. Cant, Complex chemistry DNS of n-heptane spray autoignition at high pressure and intermediate temperature conditions, Combust. Flame 160 (2013) 1254–1275.

[6] A. Krisman, E.R. Hawkes, M. Talei, A. Bhagatwala, J.H. Chen, A direct numerical simulation of cool-flame affected autoignition in diesel engine-relevant conditions, Proc. Combust. Inst. 36 (2017) 3567–3575.

[7] R.N. Dahms, G.A. Paczko, S.A. Skeen, L.M. Pickett, Understanding the ignition mechanism of high-pressure spray flames, Proc. Combust. Inst. 36 (2017) 2615–2623.

[8] Y. Minamoto, J.H. Chen, DNS of a turbulent lifted DME jet flame, Combust. Flame 169 (2016) 38–50.

[9] G. Borghesi, J. Chen, DNS of a turbulent, self-igniting n-dodecane/air jet, Bull. Am. Phys. Soc. 61 (2016).

[10] R. Dahms, G. Paczko, S.A. Skeen, L.M. Pickett, Understanding the ignition mechanism of high-pressure spray flames, Proc. Combust. Inst. 36 (2017) 2615–2623.

[11] S.M. Sarathy, C.K. Westbrook, M. Mehl, W.J. Pitz, C. Togbe, P. Dagaut, H. Wang, M.A. Oehlschlaeger, U. Niemann, K. Seshadri, P.S. Veloo, C. Ji, F.N. Egolfopoulos, T. Lu, Comprehensive chemical kinetic modeling of the oxidation of 2-methylalkanes from C7 to C20, Combust. Flame 158 (2011) 2338–2357.

[12] Y. Pei, B. Hu, S. Som, Large-Eddy simulation of an n-dodecane spray flame under different ambient oxygen conditions, J. Energy Resourc. Technol. 138 (2016) 032205-032205.

[13] Y. Pei, S. Som, P. Kundu, G.M. Goldin, Large eddy simulation of a reacting spray flame under diesel engine conditions, Report No. 0148-7191, SAE Technical Paper, 2015.

[14] Y. Pei, S. Som, E. Pomraning, P.K. Senecal, S.A. Skeen, J. Manin, L.M. Pickett, Large eddy simulation of a reacting spray flame with multiple realizations under compression ignition engine conditions, Combust. Flame 162 (2015) 4442–4455.

[15] S. Som, D. Longman, Z. Luo, M. Plomer, T. Lu, Three dimensional simulations of diesel sprays using n-dodecane as a surrogate, Fall Technical Meeting of the Eastern States Section of the Combustion Institute (2011).

[16] M.M. Ameen, Y. Pei, S. Som, Computing statistical averages from large eddy simulation of spray flames, Report No. 0148-7191, SAE Technical Paper, 2016.

[17] A. Wehrfritz, O. Kaario, V. Vuorinen, B. Somers, Large eddy simulation of n-dodecane spray flames using flamelet generated manifolds, Combust. Flame 167 (2016) 113–131.

[18] M.M. Ameen, P. Kundu, S. Som, Novel tabulated combustion model approach for lifted spray flames with large eddy simulations, SAE Int. J. Engines 9 (2016).

[19] C.K. Blomberg, L. Zeugin, S.S. Pandurangi, M. Bolla, K. Boulouchos, Y.M. Wright, Modeling split injections of ECN "Spray A" using a conditional moment closure combustion model with RANS and LES, SAE Int., J. Engines (2016) 9.

[20] C. Bekdemir, L. Somers, L. de Goey, J. Tillou, C. Angelberger, Predicting diesel combustion characteristics with large-eddy simulations including tabulated chemical kinetics, Proc. Combust. Inst. 34 (2013) 3067–3074.

[21] C. Gong, M. Jangi, X.-S. Bai, Large eddy simulation of n-Dodecane spray combustion in a high pressure combustion vessel, Appl. Energy 136 (2014) 373–381.

[22] A. Irannejad, A. Banaeizadeh, F. Jaberi, Large eddy simulation of turbulent spray combustion, Combust. Flame 162 (2015) 431–450.

[23] J. Tillou, J.B. Michel, C. Angelberger, D. Veynante, Assessing LES models based on tabulated chemistry for the simulation of Diesel spray combustion, Combust. Flame 161 (2014) 525–540.

[24] Y. Pei, E.R. Hawkes, M. Bolla, S. Kook, G.M. Goldin, Y. Yang, S.B. Pope, S. Som, An analysis of the structure of an n-dodecane spray flame using TPDF modelling, Combust. Flame 168 (2016) 420–435.

[25] Y. Pei, E.R. Hawkes, S. Kook, G.M. Goldin, T. Lu, Modelling n-dodecane spray and combustion with the transported probability density function method, Combust. Flame 162 (2015) 2006–2019.

[26] Y. Pei, E.R. Hawkes, S. Kook, A comprehensive study of effects of mixing and chemical kinetic models on predictions of n-heptane jet ignitions with the PDF method, Flow Turbul. Combust. 91 (2013) 249–280.

[27] Y. Pei, E.R. Hawkes, S. Kook, Transported probability density function modelling of the vapour phase of an n-heptane jet at diesel engine conditions, Proc. Combust. Inst. 34 (2013) 3039–3047.

[28] S.S. Pandurangi, N. Frapolli, M. Bolla, K. Boulouchos, Y.M. Wright, Influence of EGR on post-injection effectiveness in a heavy-duty diesel engine fuelled with n-Heptane, SAE Int. J. Engines 7 (2014) 1851–1862.

[29] M. Bolla, Y.M. Wright, K. Boulouchos, G. Borghesi, E. Mastorakos, Soot formation modeling of n-heptane sprays under diesel engine conditions using the conditional moment closure approach, Combust. Sci. Technol. 185 (2013) 766–793.

[30] M. Bolla, D. Farrace, Y.M. Wright, K. Boulouchos, E. Mastorakos, Influence of turbulence–chemistry interaction for n-heptane spray combustion under diesel engine conditions with emphasis on soot formation and oxidation, Combust. Theory Model. 18 (2014) 330–360.

[31] F. Tap, P. Schapotschnikow, Efficient combustion modeling based on Tabkin® CFD look-up tables: a case study of a lifted diesel spray flame, Report No. 0148-7191, SAE Technical Paper, 2012.

[32] U. Egüz, S. Ayyapureddi, C. Bekdemir, B. Somers, P. de Goey, Manifold resolution study of the FGM method for an igniting diesel spray, Fuel 113 (2013) 228–238.

[33] C. Bekdemir, L. Somers, L. de Goey, Modeling diesel engine combustion using pressure dependent flamelet generated manifolds, Proc. Combust. Inst. 33 (2011) 2887–2894.

[34] E. Abtahizadeh, P. de Goey, J. van Oijen, Development of a novel flamelet-based model to include preferential diffusion effects in autoignition of CH4/H2 flames, Combust. Flame 162 (2015) 4358–4369.

[35] C. Bajaj, M. Ameen, J. Abraham, Evaluation of an unsteady flamelet progress variable model for autoignition and flame lift-off in diesel jets, Combust. Sci. Technol. 185 (2013) 454–472.

[36] M.M. Ameen, J. Abraham, RANS and LES study of lift-off physics in reacting diesel jets, Report No. 0148-7191, SAE Technical Paper, 2014.

[37] M. Ihme, Y.C. See, Prediction of autoignition in a lifted methane/air flame using an unsteady flamelet/progress variable model, Combust. Flame 157 (2010) 1850–1862.

[38] P. Kundu, Y. Pei, M. Wang, R. Mandhapati, S. Som, Evaluation of turbulence–chemistry interaction under diesel engine conditions with multi-flamelet RIF model, Atomiz. Sprays 24 (2014).

[39] P. Kundu, Tabulated combustion model development for non-premixed flames, North Carolina State University, 2015.
[40] G. D'Errico, T. Lucchini, F. Contino, M. Jangi, X.-S. Bai, Comparison of well-mixed and multiple representative interactive flamelet approaches for diesel spray combustion modelling, Combust. Theory Model. 18 (2014) 65–88.
[41] H. Barths, C. Hasse, G. Bikas, N. Peters, Simulation of combustion in direct injection diesel engines using a eulerian particle flamelet model, Proc. Combust. Inst. 28 (2000) 1161–1168.
[42] C. Hergart, H. Barths, N. Peters, Modeling the combustion in a small-bore diesel engine using a method based on representative interactive flamelets, Report No. 0148-7191, SAE Technical Paper, 1999.
[43] H. Pitsch, H. Barths, N. Peters, Three-dimensional modeling of NOx and soot formation in DI-diesel engines using detailed chemistry based on the interactive flamelet approach, Report No. 0148-7191, SAE Technical Paper, 1996.
[44] H. Pitsch, M. Chen, N. Peters, Unsteady flamelet modeling of turbulent hydrogen-air diffusion flames, Symp. (Int.) Combust. 27 (1998) 1057–1064.
[45] S. Singh, R.D. Reitz, M.P. Musculus, Comparison of the characteristic time (CTC), representative interactive flamelet (RIF), and direct integration with detailed chemistry combustion models against optical diagnostic data for multi-mode combustion in a heavy-duty DI diesel engine, Report No. 0148-7191, SAE technical paper, 2006.
[46] H. Lehtiniemi, F. Mauss, M. Balthasar, I. Magnusson, Modeling diesel spray ignition using detailed chemistry with a progress variable approach, Combust. Sci. Technol. 178 (2006) 1977–1997.
[47] S. Keum, An improved representative interactive flamelet model accounting for evaporation effect in reaction space (RIF-ER), University of Michigan, 2009.
[48] S. Keum, H.G. Im, D.N. Assanis, A spray-interactive flamelet model for direct injection engine combustion, Combust. Sci. Technol. 184 (2012) 469–488.
[49] P. Pal, S. Keum, H.G. Im, Assessment of flamelet versus multi-zone combustion modeling approaches for stratified-charge compression ignition engines, Int. J. Engine Res. 17 (2016) 280–290.
[50] P. Kundu, T. Echekki, Y. Pei, S. Som, An equivalent dissipation rate model for capturing history effects in non-premixed flames, Combust. Flame 176 (2017) 202–212.
[51] P. Kundu, M. Ameen, U. Unnikrishnan, S. Som, Implementation of a tabulated flamelet model for compression ignition engine applications, Report No. 0148-7191, SAE Technical Paper, 2017.
[52] N. Peters, Laminar diffusion flamelet models in non-premixed turbulent combustion, Progr. Energy Combust. Sci. 10 (1984) 319–339.
[53] S. Mukhopadhyay, J. Abraham, Evaluation of an unsteady flamelet progress variable model for autoignition and flame development in compositionally stratified mixtures, Phys. Fluids 24 (2012) 075115.
[54] C. Wall, B.J. Boersma, P. Moin, An evaluation of the assumed beta probability density function subgrid-scale model for large eddy simulation of non-premixed, turbulent combustion with heat release, Phys. Fluids 12 (2000) 2522–2529.
[55] Z. Luo, M. Plomer, T. Lu, S. Som, D.E. Longman, S.M. Sarathy, W.J. Pitz, A reduced mechanism for biodiesel surrogates for compression ignition engine applications, Fuel 99 (2012) 143–153.
[56] B. Franzelli, A. Vié, M. Ihme, On the generalisation of the mixture fraction to a monotonic mixing-describing variable for the flamelet formulation of spray flames, Combus. Theory and Model. 19 (2015) 773–806.
[57] CONVERGE, Software,(Version 2.1. 0), Convergent Science, Inc., Middleton, WI, 2013.
[58] T. García-Córdova, D.N. Justo-García, B.E. García-Flores, F. García-Sánchez, Vapor−liquid equilibrium data for the nitrogen+dodecane system at temperatures from (344 to 593) K and at pressures up to 60 MPa, J. Chem. Eng. Data 56 (2011) 1555–1564.
[59] L. Qiu, R.D. Reitz, An investigation of thermodynamic states during high-pressure fuel injection using equilibrium thermodynamics, Int. J. Multiph. Flow 72 (2015) 24–38.
[60] Q. Xue, S. Som, P.K. Senecal, E. Pomraning, Large eddy simulation of fuel-spray under non-reacting IC engine conditions, Atomiz. Sprays 23 (2013).
[61] E. Pomraning, C.J. Rutland, Dynamic one-equation nonviscosity large-eddy simulation model, AIAA J. 40 (2002) 689–701.
[62] C.K. Westbrook, W.J. Pitz, O. Herbinet, H.J. Curran, E.J. Silke, A comprehensive detailed chemical kinetic reaction mechanism for combustion of n-alkane hydrocarbons from n-octane to n-hexadecane, Combust. Flame 156 (2009) 181–199.
[63] Z. Luo, S. Som, S.M. Sarathy, M. Plomer, W.J. Pitz, D.E. Longman, T. Lu, Development and validation of an n-dodecane skeletal mechanism for spray combustion applications, Combust. Theory Model. 18 (2014) 187–203.
[64] Engine Combustion Network https://ecn.sandia.gov/.
[65] N. Van Dam, S. Som, A. Swantek, C. Powell, The effect of grid resolution on predicted spray variability using multiple Large-Eddy Simulations, ASME 2016 Internal Combustion Engine Fall Technical Conference, Greenville, SC, USA (2016).
[66] S.A. Skeen, J. Manin, L.M. Pickett, Simultaneous formaldehyde PLIF and high-speed schlieren imaging for ignition visualization in high-pressure spray flames, Proc. Combust. Inst. 35 (2015) 3167–3174.
[67] W.L. Chan, H. Kolla, J.H. Chen, M. Ihme, Assessment of model assumptions and budget terms of the unsteady flamelet equations for a turbulent reacting jet-in-cross-flow, Combust. Flame 161 (2014) 2601–2613.
[68] C.-A. Hergart, H. Barths, R.M. Siewert, Modeling approaches for premixed charge compression ignition combustion, Report No. 2005-01-0218, SAE Technical Paper, 2005.
[69] B. Kerschgens, A. Vanegas, H. Pitsch, Numerical assessment of emission sources for a modified diesel engine running in PCCI mode on a mixture of gasoline and diesel, Report No. 2011-24-0014, SAE Technical Paper, 2011.
[70] S.-C. Kong, H. Kim, R.D. Reitz, Y. Kim, Comparisons of diesel PCCI combustion simulations using a representative interactive flamelet model and direct integration of CFD with detailed chemistry, J. Eng. Gas Turb. Power 129 (2006) 252–260.
[71] S. Skeen, J. Manin, L.M. Pickett, Visualization of ignition processes in high-pressure sprays with multiple injections of n-dodecane, SAE Int. J. Engines 8 (2015) 696–715.
[72] C.J. Polonowski, C.J. Mueller, C.R. Gehrke, T. Bazyn, G.C. Martin, P.M. Lillo, An experimental investigation of low-soot and soot-free combustion strategies in a heavy-duty, single-cylinder, direct-injection, Opt. Diesel Eng. (2011), doi:10.4271/2011-01-1812.